

# 1 Evaluating BC and NO<sub>x</sub> emission inventories for the Paris 2 region from MEGAPOLI aircraft measurements

3  
4 **H. Petetin<sup>1</sup>, M. Beekmann<sup>1</sup>, A. Colomb<sup>1,3</sup>, H. A. C. Denier van der Gon<sup>4</sup>,**  
5 **J.-C. Dupont<sup>5</sup>, C. Honoré<sup>6</sup>, V. Michoud<sup>1,7</sup>, Y. Morille<sup>5</sup>, O. Perrussel<sup>6</sup>, A.**  
6 **Schwarzenboeck<sup>3</sup>, J. Sciare<sup>8</sup>, A. Wiedensohler<sup>9</sup>, Q. J. Zhang<sup>1,2</sup>**

7 (1) {LISA/IPSL, Laboratoire Interuniversitaire des Systèmes Atmosphériques, UMR CNRS 7583,  
8 Université Paris Est Créteil (UPEC) et Université Paris Diderot (UPD), France.}

9 (2) {now at : ARIA, Boulogne-Billancourt, France}

10 (3) {Laboratoire de Météorologie Physique, Clermont-Ferrand, France}

11 (4) {TNO, Princetonlaan 6, 3584 CB Utrecht, The Netherlands}

12 (5) {Laboratoire de Météorologie Dynamique, Palaiseau, France}

13 (6) {AIRPARIF, Agence de surveillance de la qualité de l'air, Paris, France}

14 (7) {now at: Mines Douai, SAGE, Douai, France}

15 (8) {LSCE, Laboratoire des Sciences du Climat et de l'Environnement, CNRS-CEA-UVSQ, Gif-sur-  
16 Yvette, France}

17 (9) {Leibniz-Institute for Tropospheric Research, Leipzig, Germany}

18 Correspondence to: H. Petetin ([herve.petetin@lisa.u-pec.fr](mailto:herve.petetin@lisa.u-pec.fr))

19

## 20 **Abstract**

21 High uncertainties affect black carbon (BC) emissions and, despite its important impact on air  
22 pollution and climate, very few BC emissions evaluations are found in the literature. This paper  
23 presents a novel approach, based on airborne measurements across the Paris, France, plume,  
24 developed in order to evaluate BC and NO<sub>x</sub> emissions at the scale of a whole agglomeration. The  
25 methodology consists in integrating, for each transect, across the plume observed and simulated  
26 concentrations above background. This allows minimizing several error sources in the used model  
27 (e.g. representativeness, chemistry, plume lateral dispersion). The procedure is applied with the  
28 CHIMERE chemistry-transport model to three inventories — the EMEP inventory, and the so-called  
29 TNO and TNO-MP inventories — over the month of July 2009. Various systematic uncertainty  
30 sources both in the model (e.g. boundary layer height, vertical mixing, deposition) and in  
31 observations (e.g. BC nature) are discussed and quantified, notably through sensitivity tests. Large  
32 uncertainty values are determined in our results, which limits the usefulness of the method to rather  
33 strongly erroneous emission inventories. A statistically significant (but moderate) overestimation is

1 obtained on the TNO BC emissions and on EMEP and TNO-MP NO<sub>x</sub> emissions, as well as on the  
2 BC/NO<sub>x</sub> emission ratio in TNO-MP. The benefit of the airborne approach is discussed through a  
3 comparison with the BC/NO<sub>x</sub> ratio at a ground site in Paris, which additionally suggests a spatially  
4 heterogeneous error in BC emissions over the agglomeration.

## 5 **1 Introduction**

6 Knowledge on pollutant emissions is a key element in the field of air pollution. It provides essential  
7 information on the contribution of various source sectors to pollutant levels, which is required for  
8 targeting emission reduction measures. Emission inventories are necessary input to chemistry-  
9 transport models (CTMs) which are important tools for atmospheric research and air quality  
10 management.

11 Among the various emitted species, black carbon (BC) aerosol is a chemical compound of major  
12 importance. In air quality, it highly contributes to the health risk (Peng et al., 2009) related to fine  
13 particulate matter (PM<sub>2.5</sub>, particulate matter with aerodynamic diameter below 2.5 μm). It also plays a  
14 crucial role in the Earth's climate through the scattering and the absorption of incoming solar  
15 radiation and the subsequent change in planetary albedo (direct effect) (Schulz et al., 2006; Yu et al.,  
16 2006) and the modification of cloud properties as BC when coated with hydrophilic species acts as  
17 cloud condensation nuclei (indirect effect) (Lohmann and Feichter, 2005). The overall industrial era  
18 BC radiative forcing (including direct, semi-direct and indirect effects, as well as albedo change due  
19 to deposition on snow) is estimated at +1.1 W m<sup>-2</sup>, ranking second between the carbon dioxide  
20 (CO<sub>2</sub>, +1.56 W m<sup>-2</sup>) and methane (CH<sub>4</sub>, +0.86 W m<sup>-2</sup>) forcing (Bond et al., 2013).

21 However, high uncertainties still affect BC emission inventories making the true forcing uncertain.  
22 As a product of incomplete combustion processes, BC emissions at the global scale mainly originate  
23 from energy-related combustion (e.g. on- and off-road vehicles in transport area, biofuel and coal in  
24 residential area) and open burning (savannas and forest fires) (Bond et al., 2004, 2013; Junker and  
25 Lioussé, 2008; Lamarque et al., 2010). Global BC emissions are most recently estimated at 7.5 Tg  
26 year<sup>-1</sup>, with an uncertainty range of 2-29 Tg year<sup>-1</sup>, of which 4.8 Tg  
27 year<sup>-1</sup> originate from energy-related combustion (1.2-15 Tg year<sup>-1</sup>) (Bond et al., 2013). Most values  
28 given in the literature are included in this large (factor 10) range. Granier et al. (2011) compared  
29 inventories over the past decades at different scales. In 2005, the ratio of the highest over the lowest  
30 global BC emissions estimate is only 1.28, but higher values are given at the regional scale in  
31 Western and Central Europe, with ratios of 1.34 and 1.76, respectively. Uncertainties arise from  
32 emission factors (usually highly dependent on the conditions of use and the type of equipment),  
33 activity data and spatial distribution for some source sectors (e.g. wood burning heating). By  
34 analysing a large number of source profiles, Chow et al. (2011) found highly variable BC contents in  
35 different PM<sub>2.5</sub> emission factors, in the range of 6-37% for on-road light-duty gasoline engine

1 exhausts, 33-74% for on-road heavy-duty diesel engine exhausts, 29-61% for tire wear, 6-13% for  
2 agricultural burning, 4-33% for residential wood combustion and 3-14% for oil combustion  
3 stationary sources. Dallmann and Harley (2010) have quantified uncertainties in PM<sub>2.5</sub> emission  
4 factors for various mobile sources, such as on-road gasoline ( $\pm 45\%$ ) and on-road diesel ( $\pm 59\%$ )  
5 sources. On the contrary, the authors have estimated a much lower uncertainty in fuel consumption,  
6 around  $\pm 3$  and  $\pm 5\%$  for on-road gasoline and diesel vehicles, respectively. In the evaluation of the BC  
7 climate impact, these uncertainties on emissions contribute — among other uncertainty sources such  
8 as microphysical interactions in clouds or removal processes — to a large 95% confidence interval on  
9 the BC radiative forcing, between  $+0.17$  and  $+2.1 \text{ W m}^{-2}$  (Bond et al., 2013). It is worthwhile noting  
10 that deducing local/regional scale BC emission uncertainties (for instance over the Paris megacity)  
11 from those at global scale, appears tricky. Indeed, if on the one hand uncertainties usually increase  
12 when considering smaller domains (because of uncertainties in spatial distribution of emissions), on  
13 the other hand some uncertainty sources relevant at global scale may be reduced at European scale  
14 (e.g. minor contribution of highly uncertain open burning emissions, better constrained local activity  
15 data). This is notably the case of a megacity like Paris located in a post-industrial country where the  
16 most uncertain sources have a low contribution.

17 Compared to BC, much more efforts have been made to assess NO<sub>x</sub> emissions that in turn appear  
18 better constrained. In the inventories inter-comparison of Granier et al. (2011), the ratios between the  
19 highest and lowest NO<sub>x</sub> emissions are 1.15 at global scale, and 1.18 and 1.23 in Western and Central  
20 Europe, respectively. Due to real-time measurements, large point sources emissions are expected to  
21 be reasonably estimated in countries with mandatory emission monitoring. Concerning the traffic  
22 source, which dominates the overall emissions (particularly in summer), uncertainties are still  
23 substantial. In bottom-up inventories, these emissions are usually estimated with traffic emission  
24 models of various types and complexities. Most uncertainties arise from both activity data and  
25 emission factors. Activity data are difficult to estimate as the fleet and its technological  
26 characteristics (e.g. Euro standards) are perpetually evolving. Concerning emission factors, various  
27 techniques are available, both under controlled conditions or in real-world, and difficulties come up  
28 with their combination (see Franco et al., 2013 for a review). Compared to uncertainties previously  
29 given for PM<sub>2.5</sub> emission factors from Dallmann and Harley (2010), uncertainties for NO<sub>x</sub> emission  
30 factors are significantly lower, with values around  $\pm 27$  and  $\pm 22\%$  for on-road gasoline and on-road  
31 diesel sources, respectively. Smit et al. (2010) have reviewed results from 50 studies dealing with the  
32 validation of traffic emission models, and have pointed out a tendency to overestimate NO<sub>x</sub> emissions  
33 whatever the validation techniques (e.g. tunnel, on-board or ambient concentration studies) or the  
34 model type (e.g. average-speed, traffic situation or modal model) employed. In their critical  
35 evaluation of on-road vehicle emission inventories over the United States, Parrish (2006) indicated  
36 rather accurate NO<sub>x</sub> inventories in the 1990's but decreasing NO<sub>x</sub> emission estimates during the last

1 decade in contradiction with the tendency inferred from the evolution of NO<sub>x</sub> concentrations.  
2 Additionally, in Monte-Carlo analysis where uncertainties on NO<sub>x</sub> emissions are often considered,  
3 the two-sigma uncertainty ranges fixed for traffic NO<sub>x</sub> emissions, usually taken from the literature  
4 and/or expert judgments, vary substantially in the literature : ±80% (whatever the source) in  
5 Deguillaume et al. (2007) (deduced from the ±40% one-sigma uncertainty given in the paper),  
6 ±100% for area sources (and ±50% for point sources) in Hanna et al. (2001) (also used in Tian et al.  
7 (2010)), ±50% for area sources (and ±3% for point sources) in Napelenok et al. (2011).

8 The evaluation of these inventories still remains a critical point since emissions are generally not  
9 directly measurable. The use of CTMs for direct comparisons between measured and simulated  
10 concentrations is most of time inadequate to draw precise conclusions on emission inventories  
11 because concentrations measured at a receptor point cannot be unambiguously linked to emissions at  
12 a point aloft because of mixing processes and chemical transformations. In addition, CTMs and the  
13 meteorological input data they are using have their own uncertainties. Different alternative  
14 approaches have thus been developed. Concerning the BC emissions, useful information may be  
15 gained from their evaluation relatively to those of another compound for which uncertainty in  
16 emissions is expected to be smaller. For example Zhou et al. (2009) derived BC emissions in two  
17 Chinese megacities from CO emissions and measured BC/CO ratios at sites 10-15 km downwind of  
18 the cities. However, given the large size of these megacities, the measurement representativeness for  
19 the city emissions remains an open question. Other methods specifically assess transport patterns of  
20 emissions to the receptor point. Xu et al. (2013) have developed a method based on in-situ  
21 measurements and backward trajectory analyses to evaluate BC emissions over the North China  
22 Plain. A promising approach consists in using inverse modeling techniques, which were widely  
23 applied to NO<sub>x</sub> emissions using variational data assimilation (Mendoza-Dominguez and Russell,  
24 2000), Bayesian Monte-Carlo approaches (Deguillaume et al., 2007, Konovalov et al., 2008), Kalman  
25 Filter approaches (Napelenok et al., 2008; Gilliland and Abbitt, 2001). NO<sub>2</sub> columns retrieved by  
26 satellites (e.g. from GOME, SCIAMACHY, OMI, GOME-2) provide a valuable observational basis  
27 for many of these works because of their large data coverage. For BC, the only study using  
28 variational data assimilation we are aware of is the one of Hakami et al. (2005) that aims at better  
29 constraining BC emissions over East Asia from in-situ measurements.

30 The aim of this paper is to evaluate emission inventories at the scale of a large city. In this frame, it  
31 presents an original methodology based on airborne measurements in the city plume and chemistry-  
32 transport simulations. It is applied to BC and NO<sub>x</sub> emission inventories over the Paris megacity, with  
33 the CHIMERE model. Observations used in this study were obtained in an intensive campaign that  
34 took place in and around the city in July 2009 in the framework of the MEGAPOLI European project  
35 (Megacity : emission, urban, regional and global atmospheric pollution and climate effect, and

1 integrated tools for assessment and mitigation; [www.megapoli.info](http://www.megapoli.info)). In particular, our study relies on  
2 airborne BC measurements in the city plume, trying thus to alleviate problems of representativeness  
3 of ground based in-situ measurements. In Sect. 2, the general methodology is described. All input  
4 data, including measurement data, emission inventories, and the CHIMERE model, are described in  
5 Sect. 3. Results from both ground and airborne measurements are discussed and compared in Sect. 4.

## 6 **2 Methodology**

7 The method developed in this study aims at evaluating, at the scale of a large city, emission  
8 inventories of species that can be traced at the scale of a few hours, i.e. either a chemically inert (at  
9 the time scale considered) single compound or a conservative family of products all originating from  
10 a unique primary compound. The method is based on airborne measurements of such species in the  
11 megacity plume during the afternoon in a well-mixed convective boundary layer (BL), so that the  
12 vertical mixing can be considered as rather well established, and consequently the measured  
13 concentrations at a particular altitude as representative of concentrations in the whole BL.

14 A CTM simulation, using the inventory to be evaluated, is used to simulate tracer concentrations in  
15 the plume. For both observations and simulations, along the flight path perpendicular to the plume,  
16 tracer concentrations above regional background and within the pollution plume can be integrated.  
17 The ratio of the simulated area over the measured area corresponds to a spatially averaged emission  
18 error factor (EEF) for the agglomeration for each flight. To achieve such a calculation, the plume  
19 needs to be well distinguishable from background, which requires large enough local emissions in the  
20 city and a rather homogeneous background.

21 This method aims at reducing the influence of some errors in the CTM. By considering integrated  
22 peak areas over lateral transects across the plume, it allows minimizing the effect of some potential  
23 errors in the structure of the simulated plume, e.g. any error on lateral dispersion, reasonable errors in  
24 wind direction, and consequently to focus more on emissions. However, several potential error  
25 sources still remain, and therefore need to be carefully investigated : (i) the wind speed which  
26 directly determines the temporal window of emissions sampled during the flight, (ii) the degree of  
27 vertical mixing which determines the representativeness of the airborne measured concentrations,  
28 (iii) the wet and dry deposition of the tracer which can lead to discrepancies in the emissions factors  
29 if not well simulated by the model, and (iv) the boundary layer height that directly affects the level of  
30 concentrations. These points will all be discussed in the next sections.

31 The methodology is applied in this paper to BC and NO<sub>x</sub> emissions. As a chemically inert compound,  
32 BC can be directly used as a tracer. For the NO<sub>x</sub> compounds, as they undergo many fast chemical  
33 reactions, the NO<sub>y</sub> family gathering all reactive nitrogen species (e.g. NO<sub>x</sub>, NO<sub>3</sub>, HNO<sub>3</sub>, HONO,  
34 N<sub>2</sub>O<sub>5</sub>, PAN...) appears more conservative at the time scale of a plume, and is thus used as a tracer of  
35 NO<sub>x</sub> emissions.

## 1 **3 Input data**

### 2 **3.1 Measurement data base**

3 In the framework of the EU FP7 MEGAPOLI project (Baklanov et al., 2010), two one-month  
4 intensive campaigns (July 2009 and January/February 2010) have been organized in the Greater Paris  
5 area to better characterize organic aerosol in a large megacity. The study presented here is based on  
6 observations obtained during the summer campaign.

7 Petzold et al. (2013) have recently made some recommendations about the use of the term “BC” for  
8 black carbon, distinguishing various terminologies depending on the property used in the  
9 measurement technique: (i) the light absorbing coefficient  $\sigma_{ap}$ , or equivalent BC (EBC) if the MAC is  
10 indicated, for instruments based on light absorption, (ii) refractory BC (rBC) for instruments based  
11 on refractory properties, (iii) elemental carbon (EC) for instruments focusing on the chemical  
12 composition or the carbon content based on thermo-optical methods. So far in this paper, the term BC  
13 has been employed as a qualitative and commonly used terminology. In this section, the terminology  
14 of Petzold et al. (2013) is used.

15 Ground measurements of light absorption coefficient, EC and  $\text{NO}_x$  have been performed at the LHVP  
16 (*Laboratoire d'Hygiène de la Ville de Paris*) station (48.829°N, 2.359°E), an urban background site  
17 in the center of Paris. EC concentrations are provided by an OCEC Sunset Field instrument at a  
18 resolution of one hour. The light absorption coefficient (at a measured wavelength of 637 nm,  
19 different from the instrument nominal wavelength of 670 nm) is measured by a Multi-Angle  
20 Absorption Photometer (MAAP, Model 5012, ThermoScientific®) at a 5 min resolution, and  
21 converted into EBC with a mass-specific absorption coefficient (MAC) of  $8.8 \text{ m}^2 \text{ g}^{-1}$  derived from a  
22 linear regression between MAAP and OCEC Sunset measurements at the LHVP site ( $R^2=0.88$ ,  
23  $N=533$ , see Sect. S.1 in the Supplement, for details).  $\text{NO}_x$  observations come from a  
24 chemiluminescence monitor (AC31M, Environment SA) equipped with molybdenum oxide  
25 converters. However, an efficient conversion of many other nitrogen-containing compounds  
26 ( $\text{NO}_z = \text{NO}_y - \text{NO}_x$ ) by the molybdenum converter can lead to interferences in the  $\text{NO}_x$  concentrations  
27 (Dunlea et al., 2007). This positive artefact varies from one location to the other, depending on the  
28 relative contribution of  $\text{NO}_z$  compounds in the  $\text{NO}_y$  family. Dunlea et al. (2007) have estimated a  
29 mean overestimation of +22% in Mexico city.

30 Among the chemical data available in the Paris plume,  $\text{NO}_y$  and EBC airborne measurements aboard  
31 the French ATR-42 aircraft have been used (see Freney et al., 2013, for a detailed description of the  
32 aircraft campaign). Measurements are available for several days in July: 1, 9, 10, 13, 15 (only EBC  
33 that day), 16, 20 (only  $\text{NO}_y$ ), 21, 25, 28 (only EBC), 29 (only  $\text{NO}_y$ ).  $\text{NO}_y$  concentrations were  
34 measured at a 30 s time resolution with an instrument designed for airborne measurements that

1 consists of three Ecophysics (CLD 780 TH) analyzers in which NO is measured using ozone  
2 chemiluminescence. NO<sub>2</sub> is photolytically converted, and NO<sub>y</sub> is converted with H<sub>2</sub> in a gold covered  
3 heated oven (see Freney et al., 2013, for details). The limit of detection is 10 pptv. NO, NO<sub>2</sub> and NO<sub>y</sub>  
4 measurement uncertainties have been estimated by these latter authors to 10, 20 and 20%,  
5 respectively. The measured NO<sub>y</sub> includes the following species : NO, NO<sub>2</sub>, HNO<sub>2</sub>, HNO<sub>3</sub>, HO<sub>2</sub>NO<sub>2</sub>,  
6 N<sub>2</sub>O<sub>5</sub>, PAN, PPN and particulate nitrate. EBC particles are collected with a 50% passing efficiency  
7 aerodynamic diameter of 5.0 μm (McNaughton et al., 2007), but most soot particles are likely in the  
8 fine mode. The light absorption coefficient is measured with a 60 s time resolution from the light  
9 absorption coefficient at 650 nm provided with a Particle Soot/Absorption Photometer (PSAP)  
10 instrument (Radiance research<sup>®</sup>), corrected as in Bond et al. (1999) (see Sect. S.2 in the Supplement  
11 for details). PSAP absorption coefficient measurement uncertainties are around 20-30% (Bond et al.,  
12 1999; Virkkula et al., 2005). Absorption values are then converted into EBC concentrations using the  
13 MAC of 8.8 m<sup>2</sup> g<sup>-1</sup> already used at the LHVP site. The uncertainty related to the MAC is discussed in  
14 Sect. 4.3.4.

15 Various physical parameters are also measured in the ATR-42 aircraft at a 1 s time resolution  
16 including wind speed, wind direction and position of the aircraft (longitude, latitude, height). BL  
17 height (BLH) estimations are available at the SIRTa (*Site Instrumental de Recherche par*  
18 *Téledétection Atmosphérique*) (48.712°N, 2.208°E) (suburban background site at about 20 km in  
19 south-west of Paris) and LHVP stations. At SIRTa, they are estimated from ALS450 Leosphere  
20 backscatter lidar data at a 5 min time resolution (Haeffelin et al., 2012). At LHVP, values are  
21 estimated from CL31 ceilometer data (Haeffelin et al., 2012). Traditional meteorological parameters  
22 (wind, temperature) are also measured at SIRTa where, additionally, Leosphere wind cube lidar  
23 measurements are also available, providing wind measurements at a 10 min time resolution, each 20  
24 m from 40 to 200 m above ground level (a.g.l.).

### 25 **3.2 Emission inventories**

26 Three European anthropogenic emission inventories are evaluated in this paper, all referring to year  
27 2005:

- 28 1. The EMEP inventory (Vestreng et al., 2007), with a longitude-latitude resolution of 0.5° x  
29 0.5°.
- 30 2. An inventory developed partly in the framework of MEGAPOLI project by TNO. The  
31 inventory for the year 2005 was constructed using official emissions submitted by European  
32 countries (downloaded from EEA in 2009) in combination with a gap-filling procedure using  
33 IIASA RAINS or TNO default data. The compiled emission data were spatially distributed at  
34 a resolution of 1/8° x 1/16° degree longitude–latitude (approximately 7 x 7 km). The  
35 development of the gridded data is described in Denier van der Gon et al. (2010) and Pouliot

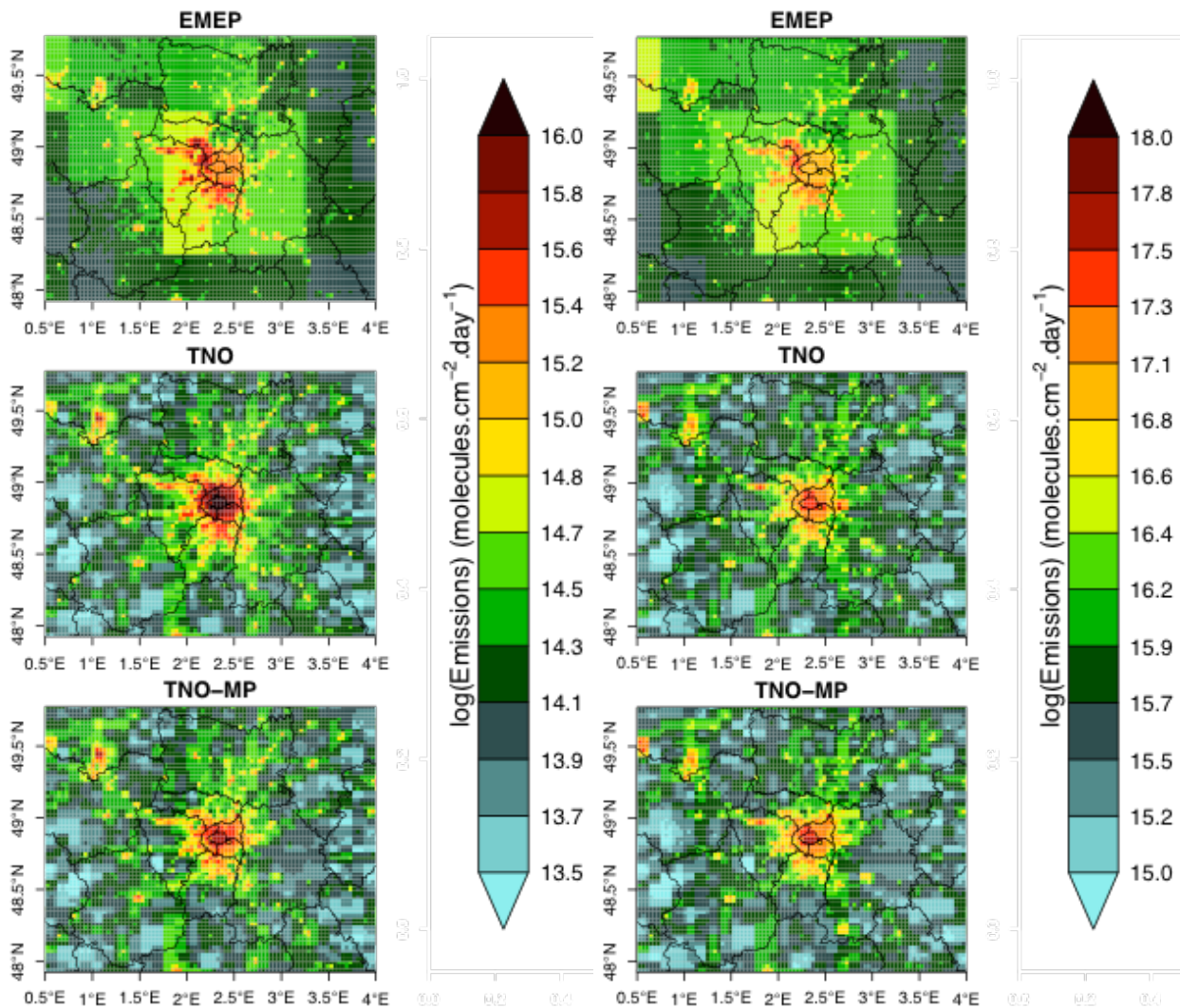
1 et al. (2012). It is the year 2005 base case inventory and also serves as a starting point for the  
2 inventory described next. In this paper it is referred to as the TNO inventory.

- 3 3. A third inventory based on the TNO inventory and with the same  $1/8^\circ \times 1/16^\circ$  longitude–  
4 latitude resolution, but incorporating bottom-up emission data over the four European  
5 megacities (Paris, London, Rhine-Ruhr and Po valley). The city emission inventories were  
6 compiled by local authorities responsible for city emissions inventories and air quality such as  
7 Airparif for Paris (Airparif, 2010). It is described in more detail by Denier van der Gon et al.  
8 (2011), and has been previously used in Zhang et al. (2013) and Timmermans et al. (2013). It  
9 will be referred as the TNO-MP (MP for MegaPoli) inventory.

10 The same EC/OC speciation table, primarily associated to the TNO inventory, is applied in all  
11 inventories. Sector-dependent factors used to derive July emissions from annual ones are reported in  
12 Table S2 in the Supplement. This table also shows the total sectorwise BC July emissions over the  
13 region for the three inventories.

14 The resolution of both TNO and TNO-MP inventories is considerably improved compared to the  
15 EMEP inventory. Despite its coarse spatial resolution, the comparison of this latter inventory with the  
16 two other refined ones remains relevant for several reasons : (i) before being applied to simulations,  
17 emissions are downscaled to the air quality model resolution, here to a 3 km horizontal resolution,  
18 using the 1x1 km-resolved GLCF (Global Land Cover Facility) landuse database (Hansen et al.,  
19 2000; Hansen and Reed, 2000), and (ii) concentrations are considered in the Paris plume, i.e. at a  
20 rather large spatial scale, which decreases the influence of such a coarse resolution in the emissions.  
21 Emissions are apportioned according to several types of landuse : urban, rural, forest, crops and  
22 maritime (Menut et al., 2013). Because of their better horizontal resolution, the evaluation of  
23 emission inventories in this paper focused mainly on the TNO and the TNO-MP inventories, the  
24 EMEP is taken as an additional reference emission inventory, as it is used in many studies in Europe.





1  
 2 Figure 1 : BC (left panel) and NO<sub>x</sub> (right panel) emissions in EMEP, TNO and TNO-MP inventories.  
 3 The spatial distribution of BC and NO<sub>x</sub> emissions in the Paris region during a typical working day in  
 4 July is given in Fig. 1 for each inventory. In order to illustrate the important differences in the spatial  
 5 distribution of emissions between inventories, one can compute for all inventories the mean  
 6 emissions of all cells within a certain distance around the LHVP site, from 0 (only the LHVP cell) to  
 7 80 km (the whole region) (see Fig. S3 in the Supplement). Relatively to TNO-MP, the EMEP  
 8 inventory BC and NO<sub>x</sub> emissions in the Paris center are relatively low, but increase further away. The  
 9 coarse resolution and the effect of the previously mentioned emission downscaling are clearly visible  
 10 on Fig. 1 for EMEP emissions, and lead to obvious discontinuities between original cells. At a large  
 11 scale, it gives the highest emissions for both compounds (and more particularly for NO<sub>x</sub> emissions).  
 12 Conversely, TNO and TNO-MP inventories display significantly higher emissions in the  
 13 agglomeration center, and lower ones further away. In summer, the TNO-MP inventory shows a quite  
 14 similar spatial emission distribution as the TNO one. In particular, major highways around Paris,  
 15 spatially unresolved or missing in the EMEP inventory, are clearly visible thanks to the refined  
 16 resolution. However, BC emissions in TNO-MP are considerably lower than in TNO in the  
 17 agglomeration. In absolute terms, discrepancies between both inventories mainly originate from road

1 transport (SNAP sector 7) and residential/tertiary (SNAP 2) sources, and in a lesser extent from  
2 waste disposal (SNAP 9), non-road transport (SNAP 8) and industrial process (SNAP 4) sources (see  
3 Table S2 in the Supplement for details). However, the highest relative discrepancies (that exceed a  
4 factor of 3) are associated to SNAP 2, 8 and 9. For sources considered as area in the top-down TNO  
5 inventory (e.g. SNAP 2 and 9), they are likely due to the distribution proxies used to downscale  
6 national totals, leading to too high emissions in Paris where the population density is very strong  
7 (Denier van der Gon et al., 2010). Concerning the SNAP 4 point sources, discrepancies can probably  
8 be explained by the use of generic capacity rules in TNO, rather than exact emissions in the TNO-  
9 MP. Both inventories are equivalent outside this region. A quite similar pattern is given for NO<sub>x</sub>  
10 emissions, except that discrepancies between both inventories in Paris are much reduced. In terms of  
11 BC/NO<sub>x</sub> emission ratios, highest values are given by the TNO inventory, followed by the EMEP one,  
12 and finally the TNO-MP one. Differences are maximum in the center of Paris, and decrease when  
13 integrating over larger areas.

14 It is worthwhile noting that as previously mentioned, both PSAP and MAAP instruments are based  
15 on the measurement of the light absorption, and observations should thus be referred as EBC.  
16 However, as emission factors and source profiles used to build emission inventories are mostly  
17 expressed as EC (Vignati et al., 2010; Chow et al., 2011; Denier van der Gon, personal  
18 communication), the simulated “BC” should be regarded as EC. An ambiguity therefore arises from  
19 comparisons between observed EBC and modeled EC since they correspond to different quantities.  
20 This point is discussed in Sect. S.1 in the Supplement and in Sect. 4.3.4. In the following, the term  
21 BC will be kept for convenience for both observations and simulations.

### 22 **3.3 CHIMERE model description**

23 In this paper, all simulations are performed with the CHIMERE CTM (Schmidt et al. 2001;  
24 Bessagnet et al., 2009; Menut et al. 2013) ([www.lmd.polytechnique.fr/chimere](http://www.lmd.polytechnique.fr/chimere)). The model was  
25 originally designed to provide (i) short-term predictions of ozone and aerosol concentrations and (ii)  
26 long-term (several years) predictions associated to emissions control scenarios. Besides research  
27 activities, it allows operational air quality survey and forecasting, and is used by different local air  
28 quality agencies in France (AASQA) and abroad, and by the French organization INERIS for daily  
29 air quality forecasting in France and Europe (PREVAIR service, [www.prevoir.org](http://www.prevoir.org)). At European  
30 scale, it is also used within the Copernicus GMES-MACC program.

31 The CHIMERE model allows simulating transport, gas-phase chemistry, some aqueous-phase  
32 reactions, size dependent aerosol species including secondary organic aerosol, dry and wet  
33 deposition. It treats coagulation, absorption as well as nucleation aerosol processes. Inorganic aerosol  
34 thermodynamic equilibrium is calculated using the ISORROPIA model (Nenes et al., 1998).

### 1 **3.4 Model configuration and simulated cases**

2 In this paper, simulations are performed during the summer MEGAPOLI campaign (July 2009) with  
3 a five-day spin-up period. Two nested domains of increasing resolution — CONT3 (0.5 x 0.5°, i.e.  
4 ~50 x 50 km, 67x46 cells) and MEG3 (0.04 x 0.027°, 120x120 cells) — are considered (see Fig. S4  
5 in the Supplement). The choice of the domains was previously explained in Zhang et al. (2013). The  
6 domain is subdivided into eight vertical layers, from ground to more than 5000 m height, with  
7 vertical resolution decreasing with altitude. The first three layers have a depth of about 40, 70 and  
8 110 m, respectively.

9 Boundary and initial conditions are taken from LMDz-INCA2 global model for gaseous species and  
10 LMDz-AERO for particulate species (Hauglustaine et al., 2004; Folberth et al., 2006). The model  
11 uses the previously described anthropogenic emission inventories, while biogenic emissions are  
12 computed with MEGAN data and parametrizations from Guenther et al. (2006). In order to  
13 investigate the influence of meteorology on results, two meteorological dataset are considered. The  
14 first has been produced with PSU/NCAR Mesoscale Meteorological model (MM5; Dudhia, 1993),  
15 performed over three nested domains with increasing resolutions of 45, 15 and 5 km respectively, and  
16 using Global Forecast System (GFS) data from the National Center for Environmental Prediction  
17 (NCEP) as boundary conditions and large scale data. The second one has been produced with the  
18 Weather Research and Forecasting model (WRF; Skamarock et al., 2005; [wrf-model.org](http://wrf-model.org)) for the  
19 same domains and resolutions. Note also that MM5 and WRF have distinct boundary layer schemes :  
20 Medium Range Forecast (MRF) for the first, and Yonsei University (YSU) for the second.

## 21 **4 Results and discussion**

22 In this section, we first evaluate meteorological input data (Sect. 4.1). A first simple approach is then  
23 applied to evaluate BC emissions against NO<sub>x</sub> ones, based on ground based measurements at the  
24 urban background LHVP site in Paris (approach n°1, Sect. 4.2). We then describe the procedure to  
25 evaluate BC emissions based on airborne measurements in the Paris plume, and present the  
26 corresponding results (approach n°2, Sect. 4.3). We finally discuss discrepancies between both  
27 methods (Sect. 4.4).

28 Statistical metrics are defined as :

29 • Mean bias:  $MB = \frac{1}{n} \sum_{i=1}^n (m_i - o_i)$  (1)

30 • Normalized mean bias:  $NMB = \frac{1}{n} \sum_{i=1}^n \frac{(m_i - o_i)}{\bar{o}}$  (2)

31 • Root mean square error:  $RMSE = \sqrt{\frac{1}{n} \sum_{i=1}^n (m_i - o_i)^2}$  (3)

1 • Normalized root mean square error: 
$$NRMSE = \frac{1}{\bar{o}} \sqrt{\frac{1}{n} \sum_{i=1}^n (m_i - o_i)^2} \quad (4)$$

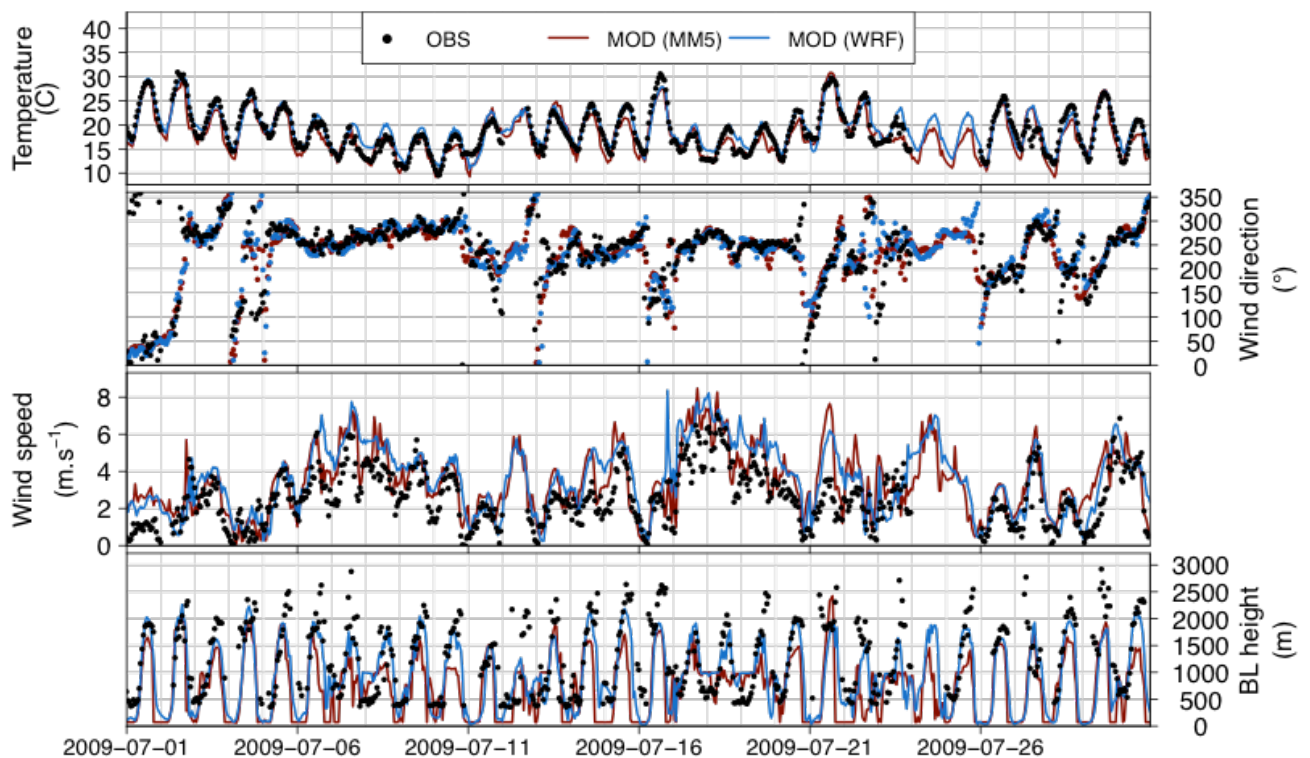
2 • Correlation coefficient: 
$$R = \frac{\sum_{i=1}^n (m_i - \bar{m})(o_i - \bar{o})}{\sqrt{\sum_{i=1}^n (m_i - \bar{m})^2 \sum_{i=1}^n (o_i - \bar{o})^2}} \quad (5)$$

3 Where  $m_i$  and  $o_i$  are the modeled and observed concentrations at time  $i$ , respectively, and  $\bar{m}$   
 4 and  $\bar{o}$  their averages over the period.

#### 5 4.1 Evaluation of meteorological data

6 In this section, meteorological input data used in CHIMERE simulations, with both MM5 and WRF  
 7 models, are evaluated against observations at surface and in altitude.

8 **Surface observations.** The Fig. 2 shows comparisons between observations and simulations for  
 9 meteorological parameters obtained at the SIRTA ground site. Statistical results are reported in the  
 10 Table 1, considering all hours as well as only the 06:00-14:00 UTC time period (designed hereafter  
 11 as morning hours), more relevant in our methodology since transport from the urban emission  
 12 sources to the aircraft location occurs in the morning and the early afternoon.



13  
 14 Figure 2 : Wind (at 10 m), temperature (at 2 m) and BLH time series in July 2009 at SIRTA site.

15 Except the first days of a continental north-easterly wind regime, the period is dominated by an  
 16 oceanic regime with west and south-west winds. The MM5 model shows a negative bias of  $-0.87^{\circ}\text{C}$   
 17 for ground temperature (reduced to  $-0.45^{\circ}\text{C}$  by considering only morning hours), and a positive one  
 18 on wind speed (+33%). BLH appears strongly underestimated, with a bias of -34%, reduced to -24%

1 during morning hours. Satisfactory correlations are found for temperature (due to diurnal cycle) and  
 2 wind speed (R around 0.8-0.9), but lower ones are obtained for BLH (around 0.5). Conversely, the  
 3 WRF model shows better results on temperature (now slightly overestimated, with a bias of +0.45°C)  
 4 and overall BLH with an underestimation reduced to -17% (and -12% during morning hours).  
 5 Correlations on this latter parameter are significantly improved compared to MM5 model (0.7 against  
 6 0.5). As one of the factors contributing to the BLH negative bias, diurnal profile comparisons (see  
 7 Fig. S5 in the Supplement) show that the transition from a convective to a stable BL in the evening  
 8 hours occurs much too early in the MM5 model, particularly at the LHVP site. This shift carries on  
 9 with WRF but is seriously reduced, which explains the better correlations.

10 Table 1 : Statistical results of MM5 (and WRF in parenthesis) considering all July hours and only the  
 11 06:00-14:00 UTC time window (N represents the proportion of available data).

Time range	Parameter	MB	NMB (%)	RMSE	NRMSE (%)	R (/)	N (%)
All hours	Temperature (°C)	-0.87 (+0.45)	-	1.94 (1.57)	-	0.92 (0.94)	90
	Wind speed (m s <sup>-1</sup> )	+0.83 (+0.99)	+33 (+39)	1.35 (1.47)	53 (58)	0.78 (0.80)	90
	BLH (m)	-440 (-224)	-34 (-17)	769 (553)	59 (43)	0.50 (0.69)	76
6:00-14:00 UTC	Temperature (°C)	-0.45 (+0.29)	-	1.76 (1.60)	-	0.92 (0.94)	89
	Wind speed (m s <sup>-1</sup> )	+1.04 (+0.71)	+35 (+24)	1.46 (1.18)	49 (39)	0.79 (0.84)	89
	BLH (m)	-345 (-176)	-24 (-12)	657 (530)	46 (37)	0.52 (0.65)	88

12

13 **Observations in altitude.** Wind lidar observations are compared with simulated wind speed in the  
 14 first model layers (the first vertical layers in CHIMERE are at 43, 118 and 248 m a.g.l.) (see Fig. S6  
 15 in the Supplement). Due to a low vertical resolution in simulations, comparisons remain qualitative.  
 16 MM5 and WRF models show quite similar patterns, but the MM5 model tends to give a higher wind  
 17 speed at all levels, including at ground. Statistical results over the 06:00-14:00 UTC time window in

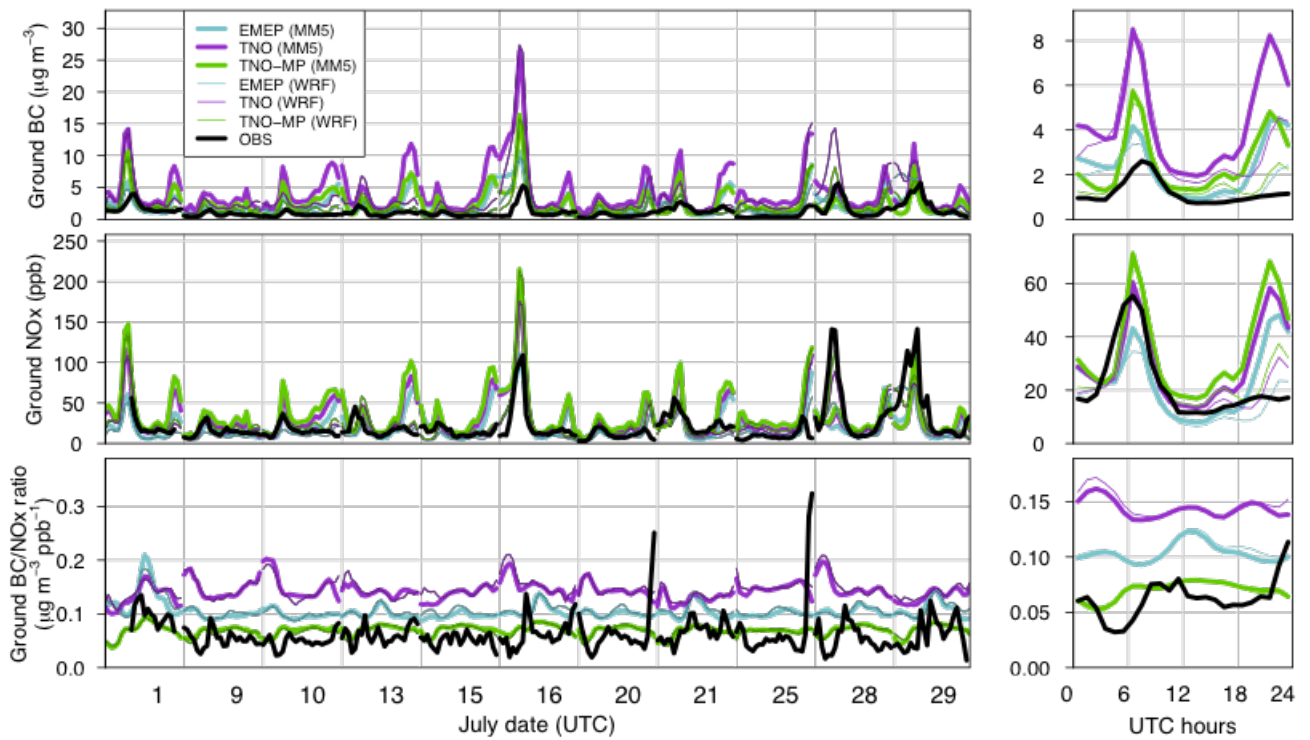
1 the 110-210 m altitude range and for the flight days are reported on Table S3 in the Supplement. In  
2 average, low negative biases and reasonable NRMSE are obtained with both MM5 and WRF models.  
3 At the daily scale, biases on wind speed remain below  $\pm 30\%$ , except the 13, 16 and 28 July  
4 (respectively the 29 July) during which one or both models give high underestimations (respectively  
5 overestimation), up to  $-46\%$  (respectively  $+27\%$  with MM5). Errors in terms of NRMSE exceed  $25\%$   
6 for all these dates, as well as during the 21 July (above  $26\%$ ) despite a low bias (error compensation  
7 between an underestimation during the first hours and overestimation during the last hours).

8 Wind speed simulation results are much better along the aircraft path (not shown), all biases  
9 remaining below  $\pm 20\%$  while NRMSE range between  $12\text{-}32\%$ . The highest biases occur the 1 and 28  
10 July, around  $-18\%$ . From a general point of view, the moderate positive bias found on wind speed at  
11 ground vanishes in altitude except at mid-altitude during specific days, leading to a noticeable  
12 decrease of the NRMSE.

#### 13 **4.2 Approach n°1 : emissions evaluation from surface measurements**

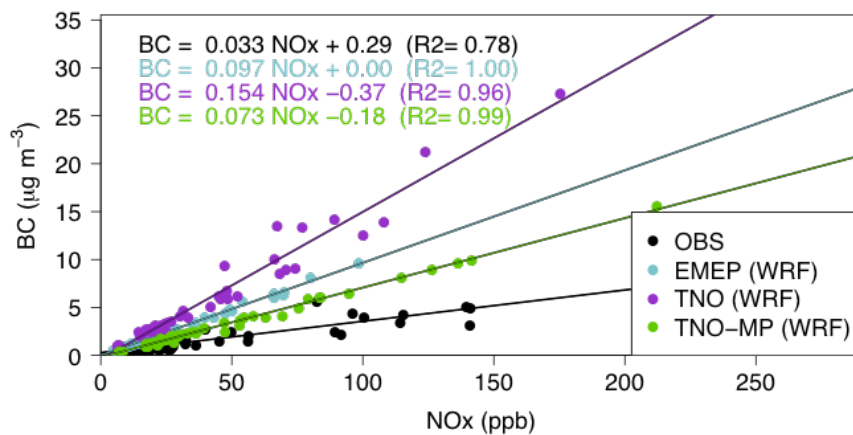
14 BC emissions can be first evaluated at ground relatively to those of  $\text{NO}_x$ , by assuming that both  
15 concentrations are proportional to their emissions close to their sources. Urban background BC and  
16  $\text{NO}_x$  concentrations, their ratio and their diurnal profiles are presented in Fig. 3, considering only  
17 flight days. Details on the evaluation of CHIMERE against observations and statistical results are  
18 given in Sect. S.3 in the Supplement. In a few words, BC is strongly overestimated, in particular with  
19 the TNO inventory and during BL transitions, the use of WRF reduces biases mainly during the late  
20 afternoon (after 18:00 UTC).  $\text{NO}_x$  is also overestimated, but mainly during the end of the day.  
21 Observed BC/ $\text{NO}_x$  ratios are rather constant ( $0.06 \mu\text{g m}^{-3} \text{ppb}^{-1}$  in average) in July except during  
22 some nights, but with a diurnal pattern showing lower values around 5 UTC and higher ones around  
23 midnight. CHIMERE also simulates rather constant ratios but with a positive bias with TNO and to  
24 less extent in EMEP inventories, while bias with TNO-MP emissions is rather small ( $< 13\%$ ).





1  
 2 Figure 3 : BC and NO<sub>x</sub> concentrations and BC/NO<sub>x</sub> ratio at LHVP urban background site during July  
 3 flight dates (left panel) and associated diurnal profiles (right panel).

4



5  
 6 Figure 4 : Observed and simulated BC versus NO<sub>x</sub> concentrations at LHVP between 05:00-08:00  
 7 UTC considering July flight days, and linear fits (lines). Only simulations with WRF meteorological  
 8 data are reported here.

9

10 We now evaluate in some more detail BC emissions relatively to NO<sub>x</sub> ones. In order to be  
 11 comparable with the airborne approach, only flight days are considered, but some results over the  
 12 whole month of July will also be indicated. It is worthwhile noting that, even if both BC and NO<sub>x</sub> are  
 13 mainly locally emitted within the Paris agglomeration, biases may be partly related to errors in  
 14 advected contributions: BC can be transported from outside (like on July 1), while some NO<sub>x</sub> may be

1 advected during the night and the early morning (when its photolytic conversion into HNO<sub>3</sub> or  
 2 HONO is less active) or released by reservoir species (e.g. PAN). NO<sub>x</sub> measurements at two rural  
 3 background stations in the south and south-east of Paris are available from the AIRPARIF network.  
 4 In average, the NO<sub>x</sub> regional background roughly accounts for 15-25% and 15-30% of the levels in  
 5 Paris for observations and simulations, respectively. From one year measurements during the  
 6 PARTICULES campaign (Bressi et al., 2013), it has been found that the BC regional background  
 7 contributes to about a third to the annual BC urban background average in Paris, and that this fraction  
 8 is probably underestimated by the CHIMERE model (Petetin et al., 2013). However, this uncertainty  
 9 source remains difficult to quantify more precisely. Additionally, NO<sub>x</sub> chemiluminescence  
 10 measurements may also include some NO<sub>z</sub> compounds (Dunlea et al., 2007), but this is not likely a  
 11 large error source since the CHIMERE model gives an average NO<sub>x</sub>/NO<sub>y</sub> ratio above 92% at the  
 12 LHVP site.

13 Given all these elements, we thus consider the BC/NO<sub>x</sub> ratio over the 05:00-08:00 UTC time  
 14 window, corresponding to rush hours where fresh NO<sub>x</sub> and BC are expected to dominate. BC versus  
 15 NO<sub>x</sub> concentrations during that time window are represented in Fig. 4. Simulated slopes of BC versus  
 16 NO<sub>x</sub> reported in Table 2 show a high overestimation with respect to observed ones for the TNO  
 17 inventory, around a factor of 4. Overestimations are reduced to a factor of 2.8 and 2.2 for EMEP and  
 18 TNO-MP inventories, respectively. Uncertainties on emission error factors (at a 95% confidence  
 19 interval) are quite the same for all inventories, around 18%, since they essentially originate from the  
 20 uncertainty on the slope deduced from observations (i.e. BC/NO<sub>x</sub> ratios are more variable in  
 21 observations than in simulations). Note also that discrepancies between BC versus NO<sub>x</sub> slopes and  
 22 BC/NO<sub>x</sub> ratios (for the latter biases remain below +136%) are due to the diurnal variability of the  
 23 measured BC/NO<sub>x</sub> ratio that shows the lowest values during the 05:00-08:00 UTC time window.  
 24 Results finally indicate an overestimation of BC emissions relative to NO<sub>x</sub> emissions, particularly in  
 25 both top-down inventories (EMEP and TNO), that is significantly reduced with local bottom-up  
 26 information integrated in the TNO-MP inventory. It is worthwhile noting that, as a burning process-  
 27 related species of long lifetime, carbon monoxide is another appropriate candidate for the evaluation  
 28 of BC emissions (Zhou et al., 2009). However, it should also be mentioned that, due to its significant  
 29 background concentrations, higher uncertainties (compared to NO<sub>x</sub>) may arise from errors in the  
 30 simulation of the regional background around Paris, even considering only rush hours.

31 Table 2 : BC versus NO<sub>x</sub> slopes and emission error factors over the 05:00-08:00 UTC time window.

Case	Flight dates		All July dates	
	BC versus NO <sub>x</sub> (µg m <sup>-3</sup> ppb <sup>-1</sup> )	Model/observations ratio [uncertainty*]	BC versus NO <sub>x</sub> (µg m <sup>-3</sup> ppb <sup>-1</sup> )	Model/observations ratio [uncertainty*]



MM5	EMEP	0.093±0.003	2.82 [18%]	0.095±0.001	2.79 [11%]
	TNO	0.135±0.009	4.09 [19%]	0.128±0.005	3.76 [11%]
	TNO-MP	0.075±0.002	2.27 [18%]	0.074±0.001	2.18 [11%]
WRF	EMEP	0.097±0.002	2.94 [18%]	0.097±0.001	2.85 [11%]
	TNO	0.154±0.010	4.67 [19%]	0.140±0.006	4.12 [11%]
	TNO-MP	0.073±0.002	2.21 [18%]	0.072±0.001	2.12 [11%]
Observations		0.033±0.006	-	0.034±0.004	-

1 \* At a 95% confidence interval.

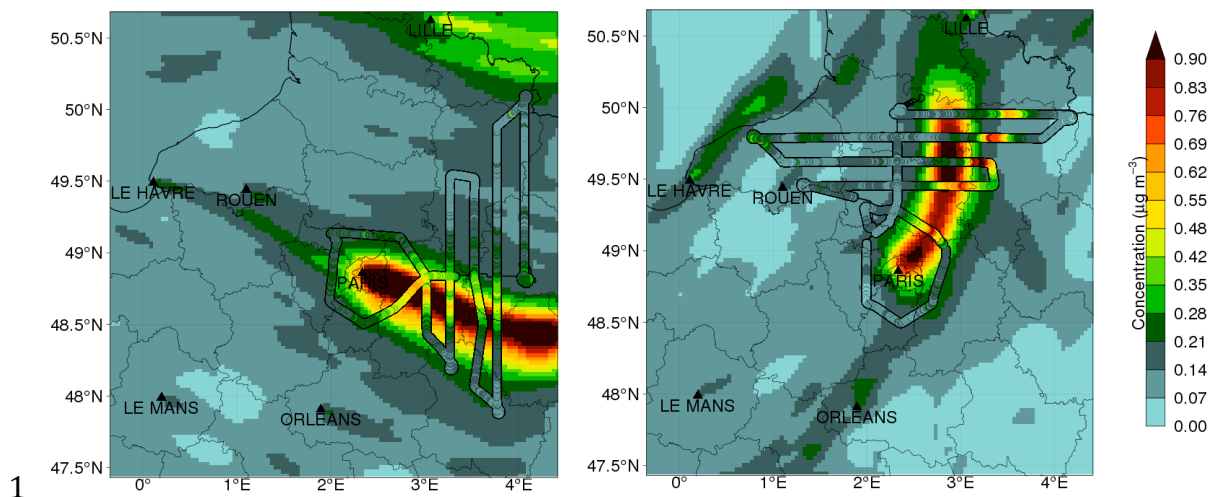
2

### 3 **4.3 Approach n°2 : emissions evaluation from airborne measurements**

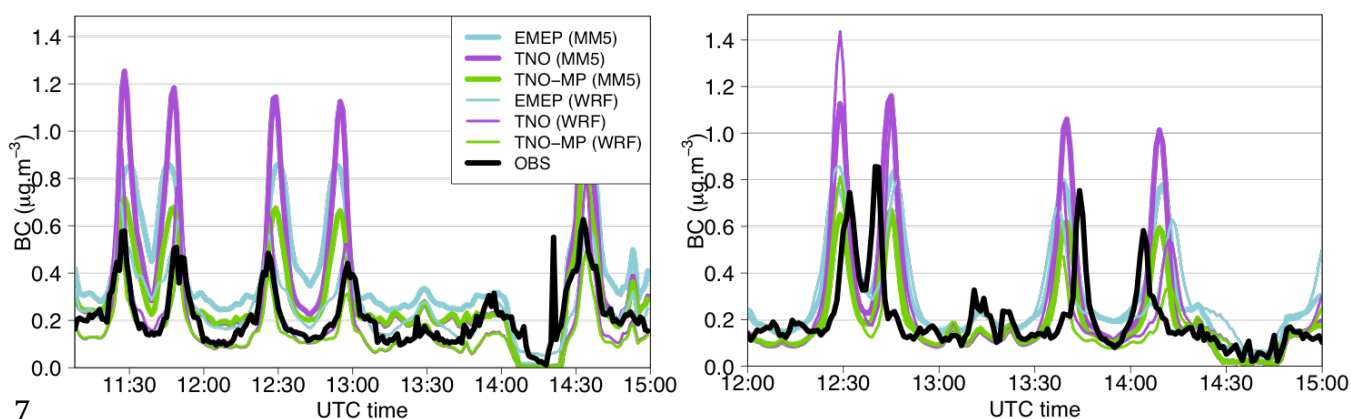
4 Given these first results obtained at ground, the alternative approach based on airborne measurements  
5 in the plume is now presented. The procedure is first described in details, and the results are then  
6 shown and their uncertainties discussed.

#### 7 **4.3.1 Procedure to compute emission error factors (EEF)**

8 As an illustration, the TNO/MM5 case for two flights on the 10 and 13 July are considered. Aircraft  
9 trajectories and BC concentrations during these days are presented in Fig. 5. As previously  
10 mentioned, the inlet used to collect BC particles is characterized by a 50% passing efficiency  
11 aerodynamic diameter of 5.0  $\mu\text{m}$ , and BC measurements are thus compared to the simulated BC  
12 concentration below 5  $\mu\text{m}$ . Time series given in Fig. 6 show a series of peaks that correspond to  
13 successive crossings of the plume (time series for all July flights are given in Fig. S7 in the  
14 Supplement). In both observations and simulations, the Paris region plume is well distinguishable  
15 against background, and peaks can thus be located on the trajectory, giving the approximate central  
16 line of the plume. Errors in the simulated wind direction lead to a shift in the spatial localization of  
17 the plume (e.g. 13 July). It is worthwhile noting that some plumes from other cities may sometimes  
18 be sampled by the aircraft. The case of the 13 July is notable: slight increases in BC concentrations in  
19 the western part of the flight track (after 13:00 UTC) correspond to plumes from Rouen and Le  
20 Havre, two industrial cities.



2 Figure 5 : Observed (along the aircraft trajectory) and modeled (in background, with the TNO-MM5  
 3 case) BC concentration for July 10 (left panel) and 13 (right panel). Paris and some other large cities are  
 4 indicated. Simulated concentrations shown here are taken at 13:00 UTC on the 4<sup>th</sup> layer that roughly  
 5 corresponds to 470-870 m height. The solid black line corresponds to the flight path outside that layer  
 6 (altitude above 870 m or below 470 m).



7  
 8 Figure 6 : Observed (in black) and simulated BC concentrations along the aircraft trajectory for July  
 9 10 (left panel) and 13 (right panel).

10 Concentration variations at the end of the flight correspond to a vertical profile up to 3 km a.g.l.  
 11 performed by the aircraft. We focus in this study on the time period during which the aircraft altitude  
 12 is rather constant (about 600 m a.g.l.). As briefly described in Sect. 2, the methodology consists in  
 13 computing for each transect the plume integral of concentrations above background, this latter being  
 14 estimated in both model and observations as the 30 percentile of concentrations in one transect (see  
 15 Fig. S8 in the Supplement). Only points above the background value are taken into account, and  
 16 additionally, some adjustments are made when winds bring plumes from other cities close to the  
 17 Paris one.

18 Given that the aircraft does not exactly cross the plume perpendicularly, but with an angle  $\alpha$  between  
 19 0 and 90° that may be different in simulations compared to real world, a correction factor of  $\sin(\alpha)$  is  
 20 thus computed and applied to each peak area. Considering that atmospheric diffusion theories predict

1 a linear relationship between point source emissions and concentrations in the plume, an emission  
 2 error factor is finally defined for each flight as the ratio of the simulated area over the observed one  
 3 (i.e. an error factor of two means an emission overestimation of 100%).

4 The emission error factor is finally defined as :

$$5 \quad EEF_{flight} = \frac{\sum_{peak} \sin(\alpha_{mod,peak}) \int_{peak} (C_{mod}(t) - C_{mod,background}) dt}{\sum_{peak} \sin(\alpha_{obs,peak}) \int_{peak} (C_{obs}(t) - C_{obs,background}) dt} \quad (6)$$

6 It is worthwhile noting that such an evaluation applies to the combination of : (i) the PM emission  
 7 inventory, (ii) the PM speciation into BC, (iii) the monthly emission factor for July and (iv) the  
 8 hourly emission profile. If uncertainties are expected to be larger on the two first elements, the two  
 9 others may also contribute to the errors. In the following discussion, it is to be kept in mind that the  
 10 reference to BC emissions aggregates all these elements.

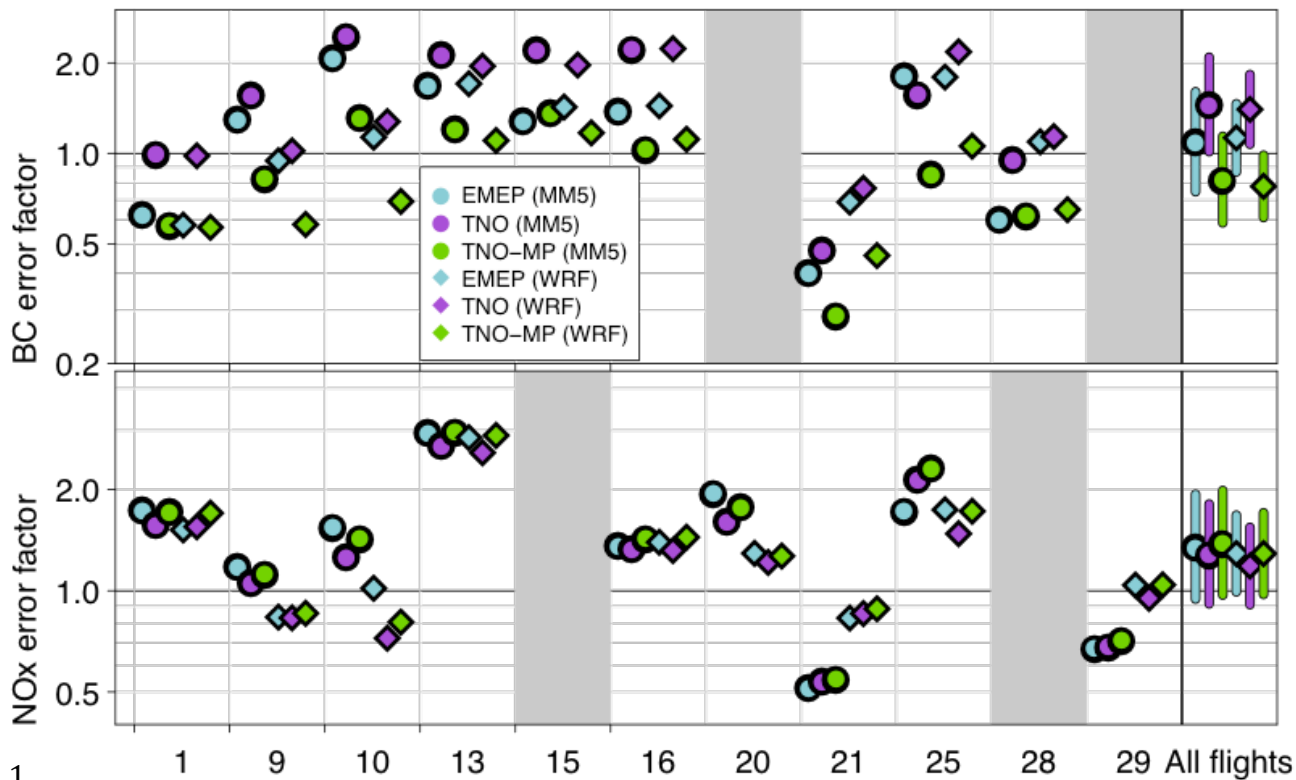
### 11 4.3.2 Results on emission error factors

12 BC and NO<sub>x</sub> emission error factors are given for each flight on Fig. 7. Average results and  
 13 confidence intervals (at a 95% confidence interval, i.e. at two sigma) are also reported, considering  
 14 errors as multiplicative:

$$15 \quad \bullet \quad \text{Mean : } \overline{EEF} = \exp\left(\frac{1}{n} \sum_{flight=1}^{nflights} \ln(EEF_{flight})\right) \quad (7)$$

$$16 \quad \bullet \quad \text{Confidence interval on the mean: } \sigma_{\overline{EEF}} = \exp\left(\frac{1}{\sqrt{n}} \sqrt{\frac{1}{n} \sum_{flight=1}^{nflights} (\ln(EEF_{flight}) - \ln(\overline{EEF}))^2}\right) \quad (8)$$

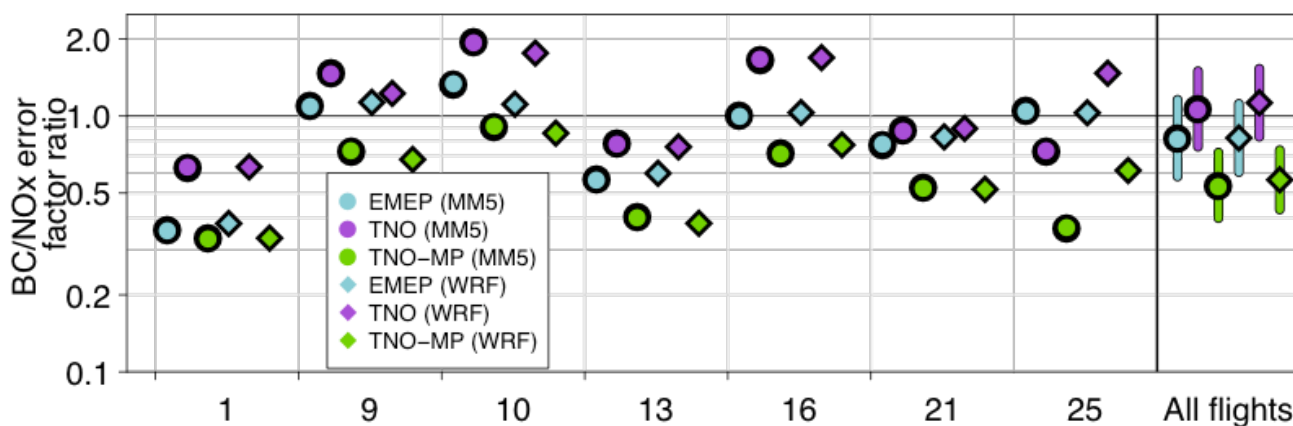
17 **BC and NO<sub>x</sub> emissions evaluation.** Mean BC emissions results are quite contrasting between  
 18 inventories and suggest in average a slight overestimation of the EMEP inventory (+9% with MM5  
 19 data), a large overestimation of the TNO inventory (+45%) and an underestimation of the TNO-MP  
 20 inventory (-18%). Results on NO<sub>x</sub> inventories show an overestimation ranging between +29 and  
 21 +39% depending on the inventory. As previously mentioned, NO<sub>y</sub> measurements may include a part  
 22 of nitrate aerosols, but including them in the model has a very slight influence on results (NO<sub>x</sub> mean  
 23 error factor changes remain below 11% for all inventories). Despite some discrepancies on specific  
 24 days between MM5 and WRF results, both give rather similar average emission biases. However, due  
 25 to the strong variability from one day to the other, uncertainties on these average values are high for  
 26 all inventories and both species, with a factor of about 1.39-1.47 for MM5 cases (at a 95%  
 27 confidence interval) but reduced to 1.27-1.31 for WRF simulations.



1

2 Figure 7 : BC (top panel) and NO<sub>x</sub> (bottom panel) emission error factors for each individual flight  
 3 (when available) and averaged emission error factor (on the right) with 95% confidence interval, for  
 4 all six simulated cases (logarithmic scale).

5 **BC/NO<sub>x</sub> emission ratio evaluation.** Ratios of BC emission error factors over NO<sub>x</sub> ones are shown in  
 6 Fig. 8 (results considering all flights are reported in Table S4 in Supplement). On average, ratios  
 7 appear underestimated in EMEP and TNO-MP inventories (-18 and -46%, respectively), while a very  
 8 low EEF (+7%) is found for the TNO inventory. However, the day-to-day variability remains as high  
 9 as that of BC and NO<sub>x</sub> taken individually, with an uncertainty on the mean around a factor 1.31-1.41.  
 10 In particular, rather small BC/NO<sub>x</sub> error factor ratios are obtained the 1, 13 and 21 July (and the 25  
 11 with MM5 meteorology), compared to the other days.



12

13 Figure 8 : BC/NO<sub>x</sub> emission error factors ratio for each individual flight and averaged for all flights  
 14 (on the right) with confidence interval, for all six simulated cases (logarithmic scale).

1 Such a high day-to-day variability both in individual compounds EFF and in their ratio was not  
2 expected, which raises the question of its origin: does it come from the real-world emissions (missing  
3 in the model emission input data), or is it induced by uncertainties in the methodology, or both? In  
4 the next subsection, the variability potentially associated to observations themselves is discussed,  
5 while the variability that may come from the methodology (e.g. model errors) will be investigated in  
6 Sect. 4.3.4.

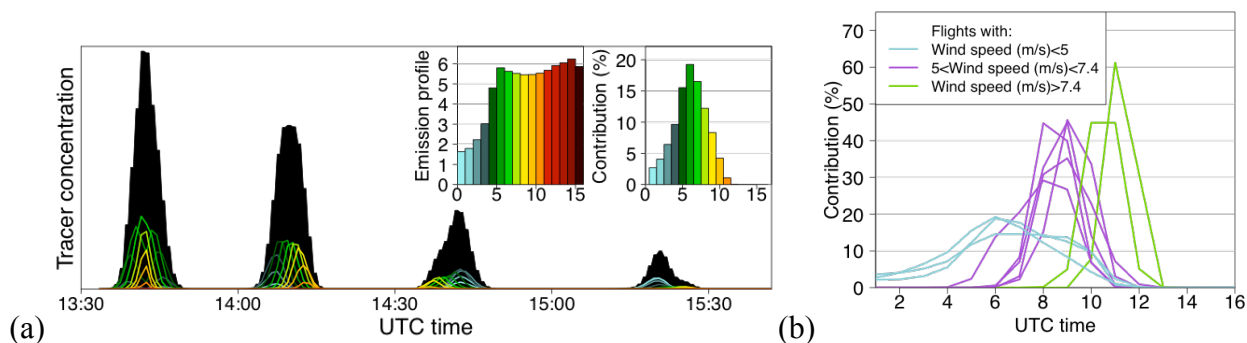
### 7 **4.3.3 Variability in observations**

8 When investigating ratios of the BC area over  $\text{NO}_y$  area for observations and simulations separately  
9 (see Fig. S9 in Supplement), one can notice that whatever the inventory, simulated BC/ $\text{NO}_x$  ratios  
10 remain rather constant from one flight to the other, leading to small uncertainties on the average  
11 value. Conversely, ratios derived from observations are much more variable, with higher values the  
12 1, 13 and 21 July compared to other days (ratios above 0.15 against 0.06-0.09, i.e. close to a factor of  
13 2), which induces uncertainties on the BC/ $\text{NO}_x$  average value in the same order of magnitude than  
14 those obtained on BC and  $\text{NO}_x$  separately. The model fails to reproduce such an enhancement during  
15 those days. The reasons for such an increase are not clear, but we can discuss some possible sources  
16 of variability.

17 **Regional background heterogeneity.** On July 1, BC measurements around Paris (and notably  
18 upwind of the city) show rather high but noisy concentrations (see Fig. S10 in Supplement), which  
19 suggests a possible heterogeneity in the BC regional background. In our methodology, a unique  
20 regional background value is estimated, based on the whole flight. In the case of a rather slender BC  
21 plume coming from the north in the axis of the Paris and adding itself to the city plume, our  
22 procedure would thus not be able to discriminate both. This may explain the high BC/ $\text{NO}_y$  ratio  
23 observed on that day.

24 **Time window of emission sampling.** Another possible source of variability in the BC/ $\text{NO}_x$   
25 emissions is related to the time window of emission sampling, as BC/ $\text{NO}_x$  diurnal profiles at LHVP  
26 show lower values during morning rush hours than in the end of the morning ( $\sim 0.04$  against  $\sim 0.07 \mu\text{g}$   
27  $\text{m}^{-3} \text{ppb}^{-1}$ ; see Fig. 3), with a noticeable day-to-day variability (see Fig. S11 in Supplement). The  
28 Paris plume sampled by the plane in the early afternoon at a distance up to 100 km from the city  
29 center originates from prior emissions, over different time windows depending on the wind speed. In  
30 order to assess which emissions are sampled in each flight, a new simulation case is run with the  
31 MM5 meteorology during the July month with 16 tracer compounds emitted each hour in a cell in the  
32 center of Paris, from 00:00 to 16:00 UTC. These inert compounds are only advected and deposited on  
33 the ground. By interpolating their concentration along each flight path, it is possible to compute the  
34 contribution of emissions at a specific hour to the overall plume. The Fig. 9a gives an illustration for  
35 July 28, for which observed wind speed at higher levels (110-210 m a.g.l.) is among the lowest (3.8

1 m s<sup>-1</sup>, see Table S3 in Supplement). Tracer emissions follow a working day emission profile. Early  
 2 morning emissions of the day (in cold colors) dominate the two last peaks, while the latter emissions  
 3 contribution (in green and hot colors) progressively increases in earlier peaks. The contribution of  
 4 emissions at a specific hour is given by the integral ratio of the associated tracer concentration over  
 5 the total concentration (black area on the figure). On this flight, the aircraft thus sample emissions  
 6 over a quite large time window (00:00-11:00 UTC), with main contributions originating from 05:00-  
 7 07:00 UTC emissions (that account for 50% of the total area). The procedure is repeated for each  
 8 flight, and contribution results for all flights are presented on Fig. 9b, colored according to their  
 9 average wind speed in altitude (Table S3 in Supplement). Due to the large daily wind speed  
 10 variability, sampling is quite different from one flight to the other. Largest windows (00:00-11:00  
 11 UTC) are sampled during the 13, 16 and 28 July flights, for which wind speed remains quite low.  
 12 Most of other flights (1, 9, 10, 20, 25 July) with intermediate wind speed have a sample window  
 13 around 06:00-11:00 UTC, while the strongest wind speeds occurring the 15 and 21 July lead to  
 14 sampling of 09:00-12:00 UTC emissions. As only late emissions are sampled on July 21, this may  
 15 explain higher ratios obtained in the plume. Unfortunately, no NO<sub>y</sub> measurements are available the  
 16 15 July with similar high wind speeds to confirm such a tendency. However, that explanation does  
 17 not apply to the 13 July flight (large window) for which the high ratio thus remains unexplained.  
 18 Note that the use of WRF is not expected to substantially modify the results obtained here with MM5  
 19 since major discrepancies between both meteorological model outputs only concern the BLH starting  
 20 from 10:00 UTC and that emission tracers are here investigated relative to each other.



21 (a) Concentration along the flight trajectory of the 16 tracers (in color line) and their total  
 22 (in black) during the 28 July flight. The emission profile gives the color associated to each tracer as  
 23 well as their emission intensity. The hourly emissions contribution over all peaks of each tracer to the  
 24 total (in terms of area) is shown in the top right corner. (b) Hourly emissions contribution to total area  
 25 for all flights. At each flight corresponds a line colored according to the mean wind speed in altitude  
 26 given in Table S3 in the Supplement. Note that, as flights occur in the afternoon, only the 16 first  
 27 hours of the day are represented.

#### 1 **4.3.4 Uncertainties of the inversion methodology**

2 The methodology used to evaluate NO<sub>x</sub> and BC emission inventories based on aircraft data over the  
3 Paris region intends to minimize several error sources : (i) the representativeness error by considering  
4 concentrations in the plume rather than at ground, (ii) modeled chemistry errors by considering inert  
5 tracer species/families, and (iii) lateral dispersion and plume direction errors by considering  
6 integrated concentrations. The high emission error factors day-to-day variability previously noticed is  
7 partly due to a variability in Paris agglomeration emissions, but such large discrepancies are not  
8 expected, and are indicative of other uncertainty sources that must be at stake, among which : (i) the  
9 wind field errors and their impact on emissions really sampled by the plane, (ii) errors in BLH and  
10 vertical mixing, (iii) errors in deposition, and finally (iv) discrepancies between EBC and EC. All  
11 these uncertainty sources are investigated in this section. Overall emission error factors uncertainties  
12 are then discussed in Sect. 4.3.5.

13 **Wind speed and emission profiles.** The methodology does not evaluate annual monthly emissions  
14 alone but also a part of the applied diurnal emission profiles (see Sect. 4.3.3) and errors on wind  
15 speed may shift the time window over which emissions are sampled (in simulations with respect to  
16 reality). This causes an additional uncertainty all the more important that the time window is narrow  
17 and temporal emission gradients are strong. In addition, wind speed errors within the city directly  
18 determine the residence time of air masses close to emission sources and thus the degree of pollutant  
19 accumulation.

20 Significant wind speed NRMSE at the SIRTA site, both at ground and at altitude levels below 200 m  
21 a.g.l. (around 40-60% and 10-60%, respectively), have been found (Sect. 4.1). These errors influence  
22 the accumulation of emitted pollutants within the city, for which uncertainties are thus probably quite  
23 important, as the accumulation time is at first order inversely proportional to the wind speed. Thus,  
24 this uncertainty in the local wind speed appears as an important source of uncertainty and variability  
25 in the day to day emission error factors. On the contrary, biases in the wind speed are reasonable, for  
26 example mostly below  $\pm 30\%$  for the wind speed at SIRTA between 100 and 200 m a.g.l., thus  
27 indicating no particular bias in emission error factors due to this error source.

28 Another uncertainty source is related to wind speed errors at higher altitudes (between the  
29 agglomeration and the measurement location), and subsequent errors on the plume advection. Given  
30 the diurnal profile of emissions and the variable emission time window sampled by the plane  
31 depending on the wind speed (Sect. 4.3.3), an error on advection would shift this time window  
32 toward earlier (respectively later) emissions in case of negative (respectively positive) biases on wind  
33 speed in altitude. This error source thus appears all the more important that the gradient in the diurnal  
34 emission profile is high in the sampled time window. Daily biases on wind speed below  $\pm 20\%$  have  
35 been found in airborne measurements along the flight path. If these uncertainties are taken as

1 representative for the average wind between the emission source and the aircraft, the typical  
2 displacements of the emission time window are less than about 1h. This would induce significant  
3 errors (say above 10%) only for time windows between 05:00 and 08:00 UTC, when the temporal  
4 gradient in emissions is strong. Thus this error source should not be of major importance to explain  
5 the variability in results.

6 **Vertical mixing.** As previously highlighted, aircraft measurements are expected to have a higher  
7 spatial representativeness than at ground, but this relies on the assumption that the vertical mixing in  
8 the BL is correctly established, so that observations obtained in the plane, at an altitude of about 600  
9 m a.g.l., can be considered as representative of those in the whole plume. The vertical heterogeneity  
10 is expected to be the highest above the city and to decrease gradually along the plume due to the  
11 turbulent mixing and the absence (or the relatively poor contribution) of fresh emissions at ground  
12 outside the city. The vertical turbulent mixing parametrization in the CHIMERE model follows the  
13 K-diffusion approach of Troen and Mahrt (1986) without counter-gradient term. Vertical fluxes are  
14 directly proportional to the vertical turbulent diffusivity coefficient ( $K_z$ ) that is bounded in the model  
15 by a minimum value of 0.01 and  $1 \text{ m}^2 \text{ s}^{-1}$  in the dry and cloudy BL, respectively, and by a maximum  
16 value of  $500 \text{ m}^2 \text{ s}^{-1}$  (Menut et al., 2013). To assess the influence of vertical mixing on results, a  
17 sensitivity test is performed by multiplying and dividing  $K_z$  values by two, as in Vautard et al.  
18 (2003). Both the dry minimum and the maximum boundaries are kept in the sensitivity test. Relative  
19 changes are shown in Fig. S12 in the Supplement. Dividing (respectively multiplying) the  $K_z$  by two  
20 leads to a moderate increase below +19% (respectively a decrease below -16%) for BC and  $\text{NO}_x$ ,  
21 while the BC/ $\text{NO}_x$  ratio does not change by more than 6%. Such small changes are quite consistent  
22 with the results obtained over the Paris agglomeration by Vautard et al. (2003) who explain the  
23 moderate impact of  $K_z$  on concentrations in altitude by the fact that a larger diffusivity increases both  
24 the incoming vertical flux from lower layers and the outgoing one toward higher layers.

25 **Boundary layer height.** The BLH is the other important parameter that requires to be correctly  
26 modeled, since it determines the volume into which the emissions will be diluted within the plume.  
27 During early afternoon, Lidar observations at SIRTa and LHVP sites have shown an underestimation  
28 by MM5 model, while significant improvements are obtained with WRF model but still with a  
29 negative bias at the SIRTa suburban site (Sect. 4.1). If such an underestimation exists in the whole  
30 flight region, it may lead to an overestimation of emission biases. However, processes are not linear,  
31 since the increased concentrations due to a lower BLH may for instance be reduced by a higher dry  
32 deposition (that depends on concentrations in lowest level). In order to assess the importance of these  
33 errors, a sensitivity test is performed with the EMEP/MM5 case by increasing the BLH by 30%  
34 (corresponding to the mean bias between 06:00-14:00 UTC). So far, simulated cases have been  
35 performed with prognostic turbulent parameters (i.e. directly taken from meteorological models).  
36 However, as the diffusivity coefficient depends on the BLH, the sensitivity test with BLH multiplied



1 by 130% is performed with the diagnostic option, in which  $K_z$  is calculated within the CTM among  
2 others as a function of the BLH. Except for some specific dates (10, 20 and 28 July), a larger BLH  
3 leads to lower concentrations and therefore decreases error factors (see relative changes in Fig. S12  
4 in the Supplement). On average, changes are around -14% for both BC and  $\text{NO}_x$ , and have rather no  
5 influence on the mean BC/ $\text{NO}_x$  ratio (-1%). Thus, the uncertainty in BLH could both contribute to the  
6 variability and bias in BC and  $\text{NO}_x$  emission error factors, while the BC/ $\text{NO}_x$  ratio is rather  
7 unaffected by these errors.

8 **Deposition.** BC and  $\text{NO}_y$  are expected to be conservative at the time scale of the flight, but they both  
9 undergo deposition. Errors in the simulated deposition and/or in the  $\text{NO}_y$  speciation (given the large  
10 differences of deposition rates among  $\text{NO}_y$  individual compounds) may impact emission biases  
11 results. Meteorological conditions indicate that wet removal is likely to be negligible over the  
12 campaign region, and the deposition is thus essentially dry. In order to assess the influence of  
13 deposition on results, a sensitivity test based on the EMEP/MM5 case is performed without any dry  
14 or wet deposition. Relative changes on BC,  $\text{NO}_x$  error factors and on their ratios are reported on Fig.  
15 S13 in the Supplement. Removing deposition increases all error factors by various amounts  
16 depending on the day. On average, error factor changes on BC and  $\text{NO}_x$  are around +7 and +16%,  
17 respectively. Without deposition, the BC/ $\text{NO}_x$  error factor ratio is decreased by -9% in average.  
18 These figures are upper limits, as errors in deposition speed are most probably less than 100%. Thus,  
19 uncertainty in deposition likely does not very much affect the error budget.

20 **Mass-specific absorption coefficient.** As previously mentioned, an additional uncertainty may arise  
21 from the comparison between EBC (observations) and EC (emissions and simulations), through the  
22 MAC value used to convert absorption coefficients into EBC concentrations. Airborne PSAP EBC  
23 concentrations have been obtained considering a constant MAC of  $8.8 \text{ m}^2 \text{ g}^{-1}$  deduced from  
24 measurements at the LHVP site in Paris (see Sect. S.1 in the Supplement). The relevancy of  
25 comparisons performed in this study with the simulated EC thus relies on the hypothesis that this  
26 MAC determined in the Paris center is valid at the scale of the whole agglomeration, and that it  
27 remains constant along the flight. This is supported by the MAC value estimated in winter 2009 by  
28 Sciare et al. (2011) at a suburban site at 20 km in the south-west of Paris that remains in the same  
29 order of magnitude than the one obtained here in the Paris center ( $7.3 \pm 0.1 \text{ m}^2 \text{ g}^{-1}$ ). Actually, during  
30 that winter season, but one year later, single particle Aerosol Time-Of-Flight Mass Spectrometer  
31 observations performed at the LHVP site during the MEGAPOLI winter campaign have shown a  
32 majority of already internally mixed BC particles (with a shell of organic material and secondary  
33 inorganic compounds) (Healy et al., 2012). Therefore, the MAC variations along the flight are  
34 expected to be reasonable. This is also supported by the analysis of BC/ $\text{NO}_y$  ratios obtained from  
35 aircraft observations that does not show any significant increase with distance from Paris, which  
36 would be expected if the MAC value increased with distance from the emission source. Additionally,

1 it is worthwhile noting that direct measurements of the MAC enhancement by Cappa et al. (2012)  
2 have recently shown a very low enhancement between near source and more distant values, only by  
3 around +6%, onboard a ship along the California coast (CalNex campaign) and at a ground site  
4 located at 14 km of Sacramento (Carbonaceous Aerosols and Radiative Effects Study, CARES  
5 campaign). Considering the previous MAC estimations in the Paris region — 7.3 and 12.0  $\text{m}^2 \text{g}^{-1}$  by  
6 Sciare et al. (2011) and Lioussé et al. (1993), respectively — the uncertainty associated to our MAC  
7 value ( $8.8 \text{ m}^2 \text{g}^{-1}$ ) is roughly estimated at 30%.

#### 8 **4.3.5 Statistical significance of the results**

9 Results obtained for each compound in Sect. 4.3.2 consist in mean error factors and rather large  
10 confidence intervals that result from (i) uncertainties associated to the day-to-day variability which is  
11 not included in the model input data (beyond the temporal dependence on the month and the day of  
12 the week), (ii) measurement uncertainties and (iii) uncertainties in the methodology (conditioned by  
13 error sources in the model).

14 The first ones are difficult to quantify but can reasonably be considered as random. Also  
15 measurement uncertainties are probably mostly random, but may include a part of systematic  
16 uncertainties. In order to be conservative, they are assumed entirely as systematic. Uncertainties in  
17 the methodology have been discussed in previous sections, notably through various sensitivity tests  
18 on deposition, boundary layer height and the turbulence diffusivity coefficient. Results have shown  
19 that all investigated uncertainties in the model influence mean emission error factors, and their  
20 variability. They have therefore a systematic and a random part, which we could estimate in the  
21 previous sensitivity tests. These tests have shown a significant day-to-day variability, which suggests  
22 that they are probably partly random and may thus explain most of the day-to-day variability  
23 obtained in first results (Sect. 4.3.2). It appears rather tricky (and uncertain) to explain all  
24 discrepancies between individual flight results on a quantitative basis, notably due to the fact that  
25 several uncertainty sources are potentially combined. In spite of that, the choice is made to replace  
26 the uncertainty obtained in Sect. 4.3.2 by a combination of all the systematic uncertainties estimated  
27 in the previous subsection. Results of individual and the derived overall systematic uncertainty are  
28 reported in Table 3, as well as final confidence intervals on our estimation of emission error factors.

29 Table 3: Systematic two-sigma uncertainties on BC and  $\text{NO}_x$  error factors and BC/ $\text{NO}_x$  error factor  
30 ratio from various sources, and associated confidence intervals on average emission error biases for  
31 the three inventories.

Uncertainty source	BC	$\text{NO}_x$	BC/ $\text{NO}_x$
Boundary layer height	14%	14%	1%

Vertical mixing	17%	19%	6%
Deposition	7%	16%	9%
Mass-specific absorption coefficient	30%	-	30%
NO <sub>y</sub> and absorption coefficient measurement	30%	20%	36%
Overall uncertainty	48%	35%	48%

1 Confidence intervals (at a 95% confidence interval) on average emission error biases deduced from  
2 the overall uncertainty are reported in Table 4. For NO<sub>x</sub> emissions, positive biases are found in all  
3 inventories. Considering the 95% confidence intervals, the bias in the TNO inventory appears  
4 statistically insignificant, which may not be the case in both EMEP and TNO-MP inventories for  
5 which a slight overestimation remains probable (due to a confidence interval lower bound of -4%,  
6 thus very close to zero). These are in the range of the 35% agreement found for NO<sub>x</sub> emissions in  
7 Paris during the ESQUIF project in summer 1999 by Vautard et al. (2003) also based on airborne  
8 measurements and CHIMERE simulations, but using an alternative method, and an older emission  
9 inventory prepared by AIRPARIF. Through an inverse modeling exercise based on satellite NO<sub>2</sub>  
10 columns, Konovalov et al. (2006) have obtained a similar 30% overestimation of the EMEP  
11 inventory in the Paris area. Through another inverse emission modeling based on ground  
12 measurements over the Paris region, Deguillaume et al. (2007) have found no significative bias, but  
13 an uncertainty of about ±20 %. Note that these studies were performed using different emission  
14 inventories. Given the uncertainties, the NO<sub>x</sub> emissions positive bias around 20-30% found here in  
15 most of the inventories does not appear as significant.

16 Table 4 : Confidence intervals on average emission error biases for the three inventories.

Inventory	BC	NO <sub>x</sub>	BC/NO <sub>x</sub>
EMEP	+12% (-24%; +66%)	+29% (-4%; +74%)	-18% (-45%; +22%)
TNO	+40% (-6%; +108%)	+18% (-12%; +59%)	+13% (-24%; +67%)
TNO-MP	-23% (-48%; +15%)	+29% (-4%; +74%)	-44% (-62%; -17%)

17 Also both the positive bias (around +12%) of EMEP and the negative one (around -23%) of TNO-  
18 MP BC emissions are not significant, while the 95% confidence interval of the TNO inventory  
19 indicates a probable overestimation of BC emissions in that inventory. As previously mentioned in

1 Sect. 3.2, the overestimation of BC emissions in the TNO inventory can probably be explained by the  
2 spatial distribution procedure that concentrates too large emissions in the city. For example, using  
3 population density as a proxy implies the assumption of constant per capita emissions over the  
4 country which might lead to an overestimation of urban BC emissions as discussed in Timmermans  
5 et al., (2013) and references therein. At this stage, it is to be emphasized that discrepancies between  
6 EMEP and TNO BC results are mostly related to differences in their spatial resolution since input  
7 data for national totals are similar. Accordingly, Paris region total emissions in July are quite similar  
8 in both EMEP and TNO inventories (as shown in Table S2 in Supplement). However, at the scale of  
9 the Paris agglomeration, total emissions in both inventories do show discrepancies, TNO emissions  
10 being more concentrated in the city due to its finer resolution while the EMEP emissions spill over in  
11 rural areas of Paris region due to their coarser resolution (see Sect. 3.2). Therefore, to our sense, the  
12 better results obtained with EMEP have to be interpreted with caution. Potential errors in the  
13 distribution of BC emissions are partly avoided in the TNO-MP inventory which follows a more (but  
14 not fully) bottom-up approach. Concerning the BC/NO<sub>x</sub> emission ratio, the only statistically  
15 significant negative bias concerns the TNO-MP inventory, while results for both EMEP and TNO  
16 inventories suggest error compensation in BC and NO<sub>x</sub> emissions, leading to a satisfactory estimation  
17 of BC/NO<sub>x</sub> emission ratio. It is worthwhile reminding that, in this study, the same BC speciation  
18 table (primarily built for the TNO inventory) has been used in all inventories in order to be  
19 consistent, but the use of a more specific speciation to the Paris region would maybe change these  
20 results, in particular for the TNO-MP inventory in which a part of the bottom-up information is lost  
21 through the use of a constant BC speciation in this study. Another point to be mentioned concerns the  
22 emissions inter-annual variability that adds an additional uncertainty (similar for all inventories) due  
23 to the comparison of observations from 2009 with inventories built for 2005.

24 To our knowledge, a BC emissions evaluation as presented here has not yet been attempted at the  
25 scale of a large megacity, and uncertainties estimated at the global or regional scale are difficult to  
26 extrapolate to an agglomeration. For comparison, through their adjoint inverse modeling exercise  
27 over Asia, Hakami et al. (2005) have found quite consistent total assimilated and base case BC  
28 emissions over Asia, but have underlined higher discrepancies at regional scale, with major errors  
29 over Japan, northern and southern China of about a factor  $\pm$  two.

#### 30 **4.4 Surface versus airborne results : representativeness issues**

31 Results obtained at ground in Paris show a high overestimation of the BC/NO<sub>x</sub> ratio in the TNO (~  
32 factor 4) and EMEP (~ factor 3) inventories, and at a lesser extent in TNO-MP (~ factor 2). This is  
33 not consistent with results obtained in the plume where the BC/NO<sub>x</sub> emission ratio appears highly  
34 underestimated in TNO-MP (while errors are lower for EMEP and TNO). Several reasons may at  
35 least partly explain these discrepancies between ground and airborne results. The main one is  
36 probably the difference of representativeness between both approaches, ground concentrations being

1 influenced by emissions in the vicinity of the LHVP station, while concentrations in the plume  
2 integrate emissions at a much larger scale (the whole agglomeration). In order to assess the LHVP  
3 site representativeness, a simulation with spatially traced emissions around that site is performed over  
4 a few days (see Sect. S.4 in the Supplement). LHVP concentrations appear mainly influenced by  
5 close emissions, with a contribution of 50-85% from emissions within a radius of 6 km around the  
6 site. Conversely, beyond a radius of 21 km (which still covers the agglomeration), emissions  
7 contribute to less than 10%. These contributions are quite variable depending on the wind field, the  
8 importance of close emissions increasing with stagnant conditions. Since BC and NO<sub>x</sub> emissions as  
9 well as their ratio are highly heterogeneous over the whole Paris region (see Sect. 3.2 and Fig. S3 in  
10 the Supplement), results obtained at the LHVP site thus cannot be representative for the whole  
11 agglomeration, but probably only for its central part.

12 Additionally, the previous tracer experiment takes into account neither the sub-grid emissions  
13 heterogeneity at a resolution of 3x3 km (e.g. a park and a stretch of the Paris ring road are included in  
14 the LHVP cell) nor sub-cell processes, caused by the high complexity of urban environments (e.g.  
15 street canyons, building-induced turbulence). The LHVP spatial representativeness may thus be even  
16 lower. Working at the plume scale strongly reduces these limitations since (i) all emissions within the  
17 agglomeration end up in the plume, and (ii) mixing during a few hours of transport from the source  
18 regions to the measurement locations is expected to significantly increase the concentration  
19 representativeness.

20 This would therefore suggest that the best BC/NO<sub>x</sub> emission ratio is given by the TNO-MP inventory  
21 in the Paris center, while it highly underestimates the ratio at the scale of the whole agglomeration,  
22 contrary to the TNO inventory which gives better results. Compared to TNO-MP, NO<sub>x</sub> emissions in  
23 TNO are quite similar while BC ones are higher and more concentrated in the center of Paris.

## 24 **5 Conclusion**

25 Black carbon (BC) emissions are still highly uncertain, and very few studies have attempted to  
26 evaluate their inventories. This paper presents an original approach, based on airborne measurements  
27 across the Paris plume, developed in order to evaluate BC and NO<sub>x</sub> emissions at the scale of the  
28 whole agglomeration. It is applied to three emission inventories (EMEP, TNO, TNO-MP). In order to  
29 assess the benefit of such a methodology, BC/NO<sub>x</sub> ratios at the LHVP ground site in Paris are first  
30 investigated. Over the whole July month, they show a significant (at a 95% confidence interval)  
31 overestimation in all inventories with biases ranging between a factor of 2 in TNO-MP and a factor  
32 of 4 in TNO. On average, results obtained from July airborne observations give an overestimation of  
33 NO<sub>x</sub> emissions around +20-30% for all inventories, a moderate bias around +12 and -23% for EMEP  
34 and TNO-MP BC emissions, respectively, but a higher positive bias of +40% for TNO BC inventory.  
35 However, these results present an unexpected high day-to-day variability (up to a factor of about 3).

1 Low biases are also obtained on BC/NO<sub>x</sub> emission ratio for EMEP and TNO inventories (-18 and  
2 +13%, respectively), contrary to the TNO-MP inventory that shows an underestimation of -44%.

3 Various uncertainty sources in the methodology are investigated through sensitivity tests — wind  
4 field errors, boundary layer height, vertical mixing, deposition, BC nature (equivalent BC versus  
5 elemental carbon) — and are likely to explain this variability. Results of these tests are used to derive  
6 a systematic uncertainty between 35 and 48% on emission error factors. This suggests that a  
7 moderate overestimation of NO<sub>x</sub> July emissions in EMEP and TNO-MP inventories is statistically  
8 probable. Biases found in EMEP and TNO-MP BC emissions are not significant. However, the  
9 overestimation in TNO BC emissions does appear as significant. It is probably due to the distribution  
10 proxies used to downscale national total emissions that concentrate too large emissions in a highly  
11 populated area such as Paris with lower per capita emissions. The BC/NO<sub>x</sub> emission ratio appears  
12 underestimated in the TNO-MP inventory, while non-significant biases are obtained with both EMEP  
13 and TNO inventories. While discrepancies between EMEP and TNO inventories are likely due to  
14 differences in spatial resolutions and allocation, the ones between TNO and TNO-MP do illustrate  
15 the distinction between bottom-up and top-down approaches. Results obtained at a ground based site  
16 in Paris are not consistent with those obtained in the plume, due to the fact that surface measurements  
17 are representative only for an area surrounding the LVHP site by a few kilometers while emissions  
18 from the whole agglomeration are sampled in the Paris plume.

19 Finally, best estimations of BC and NO<sub>x</sub> emission biases thus do not exceed  $\pm 40\%$ , which appears as  
20 rather moderate considering the numerous uncertainties at stake in the construction of an inventory.  
21 Due to methodological uncertainties in the same order of magnitude, assessing the significance of all  
22 these results remains difficult. However, the methodology does succeed in highlighting some  
23 statistically significant biases and in particular, for BC or NO<sub>x</sub> emissions or for the BC/NO<sub>x</sub> ratio, at  
24 least one of the three inventories has been proven as very probably biased. It is worthwhile noting  
25 that the methodology used in this study not only evaluates an inventory by itself but also a particulate  
26 matter speciation table and a temporal disaggregation (monthly and diurnal) that are also subject to  
27 potential errors.

28 To our knowledge, this study is one of the most comprehensive ones to evaluate BC emissions at the  
29 scale of a large megacity. The comparison of aircraft- and ground-based results has given an  
30 interesting insight on the potential error compensation in the spatial allocation of BC emissions over  
31 a large agglomeration. In the framework of the PRIMEQUAL PREQUALIF project, a dense BC  
32 network of 14 stations (of various typologies, e.g. rural, urban, traffic) has been installed over the  
33 Paris region. It will allow a better characterization of the BC spatial distribution over the  
34 agglomeration, and in the line of this, an interesting outlook would thus be to compare it to the  
35 simulated spatial distribution constrained by emission inventories.

1

## 2 **Acknowledgements**

3 The research leading to these results has received funding from the European Union's Seventh  
4 Framework Programme FP/2007-2011 under grant agreement no. 212520. The authors also  
5 acknowledge the ANR through the MEGAPOLI PARIS and ADEME and LEFE through the  
6 MEGAPOLI France project for their financial support. This work is funded by a PhD DIM (*domaine*  
7 *d'intérêt majeur*) grant from the Ile-de-France region. We would like to thank the two anonymous  
8 referees for their valuable comments on this work.

## 9 **References**

- 10 Airparif : Inventaire des émissions en Ile-de-France, Méthodologie et résultats année 2005 (in  
11 french), 2010.
- 12 Baklanov, A., Lawrence, M., Pandis, S., Mahura, A., Finardi, S., Moussiopoulos, N., Beekmann, M.,  
13 Laj, P., Gomes, L., Jaffrezo, J.-L., Borbon, A., Coll, I., Gros, V., Sciare, J., Kukkonen, J.,  
14 Galmarini, S., Giorgi, F., Grimmond, S., Esau, I., Stohl, A., Denby, B., Wagner, T., Butler, T.,  
15 Baltensperger, U., Builtjes, P., van den Hout, D., van der Gon, H. D., Collins, B., Schluenzen,  
16 H., Kulmala, M., Zilitinkevich, S., Sokhi, R., Friedrich, R., Theloke, J., Kummer, U., Jalkinen,  
17 L., Halenka, T., Wiedensholer, A., Pyle, J., and Rossow, W. B. : MEGAPOLI : concept of  
18 multi-scale modelling of megacity impact on air quality and climate, *Advances in Science and*  
19 *Research*, 4, 115–120, 2010.
- 20 Bessagnet, B., Menut, L., Curci, G., Hodzic, A., Guillaume, B., Liousse, C., Moukhtar, S., Pun, B.,  
21 Seigneur, C., and Schulz, M. : Regional modeling of carbonaceous aerosols over Europe -  
22 focus on secondary organic aerosols, *J. Atmos. Chem.*, 61, 175–202, 2009.
- 23 Bond, T. C., Anderson, T. L., and Campbell, D. : Calibration and Intercomparison of Filter-Based  
24 Measurements of Visible Light Absorption by Aerosols, *Aerosol Sci. Tech.*, 30, 582–600,  
25 1999.
- 26 Bond, T. C., Streets, D. G., Yarber, K. F., Nelson, S. M., Woo, J.-H., Klimont, Z.: A technology-  
27 based global inventory of black and organic carbon emissions from combustion, *J. Geophys.*  
28 *Res.*, 109, D14 203, 2004.
- 29 Bond, T. C., Doherty, S. J., Fahey, D. W., Forster, P. M., Berntsen, T., DeAngelo, B. J., Flanner, M.  
30 G., Ghan, S., Kärcher, B., Koch, D., Kinne, S., Kondo, Y., Quinn, P. K., Sarofim, M. C.,  
31 Schultz, M. G., Schulz, M., Venkataraman, C., Zhang, H., Zhang, S., Bellouin, N., Guttikunda,  
32 S. K., Hopke, P. K., Jacobson, M. Z., Kaiser, J. W., Klimont, Z., Lohmann, U., Schwarz, J. P.,  
33 Shindell, D., Storelvmo, T., Warren, S. G., and Zender, C. S. : Bounding the role of black  
34 carbon in the climate system : A scientific assessment, *J. Geophys. Res.-Atmos.*, 118, 1–173,  
35 2013.

- 1 Bressi, M., Sciare, J., Ghersi, V., Bonnaire, N., Nicolas, J. B., Petit, J.-E., Moukhtar, S., Rosso, A.,  
2 Mihalopoulos, N., and Féron, A. : A one-year comprehensive chemical characterisation of fine  
3 aerosol (PM<sub>2.5</sub>) at urban, suburban and rural background sites in the region of Paris (France),  
4 *Atmos. Chem. Phys.*, 13, 7825–7844, 2013.
- 5 Cappa, C. D., Onasch, T. B., Massoli, P., Worsnop, D. R., Bates, T. S., Cross, E. S., Davidovits, P.,  
6 Hakala, J., Hayden, K. L., Jobson, B. T., Kolesar, K. R., Lack, D. A., Lerner, B. M., Li, S.-M.,  
7 Mellon, D., Nuaaman, I., Olfert, J. S., Petäjä, T., Quinn, P. K., Song, C., Subramanian, R.,  
8 Williams, E. J., and Zaveri, R. A. : Radiative absorption enhancements due to the mixing state  
9 of atmospheric black carbon, *Science (New York, N.Y.)*, 337, 1078–1081, 2012.
- 10 Chow, J. C., Watson, J. G., Lowenthal, D. H., Antony Chen, L.-W., and Motallebi, N. : PM<sub>2.5</sub> source  
11 profiles for black and organic carbon emission inventories, *Atmos. Environ.*, 45, 5407–5414,  
12 2011.
- 13 Dallmann, T. R. and Harley, R. A. : Evaluation of mobile source emission trends in the United States,  
14 *J. Geophys. Res.*, 115, D14 305, 2010.
- 15 Deguillaume, L., Beekmann, M., and Menut, L. : Bayesian Monte Carlo analysis applied to regional-  
16 scale inverse emission modeling for reactive trace gases, *J. Geophys. Res.*, 112, D02 307, 2007.
- 17 Denier van der Gon, H.A.C., Visschedijk, A. van der Brugh, H. Dröge, R. : A high resolution  
18 European emission data base for the year 2005. A contribution to UBA-Projekt PAREST:  
19 Particle Reduction, Strategies, TNO-034-UT-2010-01895\_RPT-ML, 2010.
- 20 Denier van der Gon, H.A.C., Beevers, S., Al D’Allura, et al. : Discrepancies between top-down and  
21 bottom-up emission inventories of megacities: the causes and relevance for modeling  
22 concentrations and exposure. In: Steyn, D.G., Castelli, S.T. (Eds.), *NATO Science for Peace  
23 and Security Series C: Environmental Security*, vol. 4, 2011.
- 24 Dudhia, J. : A Nonhydrostatic Version of the Penn State-NCAR Mesoscale Model : Validation Tests  
25 and Simulation of an Atlantic Cyclone and Cold Front, *Mon. Weather Rev.*, 121, 1493–1513,  
26 1993.
- 27 Dunlea, E. J., Herndon, S. C., Nelson, D. D., Volkamer, R. M., San Martini, F., Sheehy, P. M.,  
28 Zahniser, M. S., Shorter, J. H., Wormhoudt, J. C., Lamb, B. K., Allwine, E. J., Gaffney, J. S.,  
29 Marley, N. A., Grutter, M., Marquez, C., Blanco, S., Cardenas, B., Retama, A., Ramos  
30 Villegas, C. R., Kolb, C. E., Molina, L. T., and Molina, M. J. : Evaluation of nitrogen dioxide  
31 chemiluminescence monitors in a polluted urban environment, *Atmos. Chem. Phys.*, 7, 2691-  
32 2704, 2007.
- 33 Folberth, G. A., Hauglustaine, D. A., Lathière, J., and Brocheton, F. : Interactive chemistry in the  
34 Laboratoire de Météorologie Dynamique general circulation model : model description and  
35 impact analysis of biogenic hydrocarbons on tropospheric chemistry, *Atmos. Chem. Phys.*, 6,  
36 2273–2319, 2006.



- 1 Franco, V., Kousoulidou, M., Muntean, M., Ntziachristos, L., Hausberger, S., and Dilara, P. : Road  
2 vehicle emission factors development : A review, *Atmos. Environ.*, 70, 84–97, 2013.
- 3 Freney, E. J., Sellegri, K., Canonaco, F., Colomb, A., Borbon, A., Michoud, V., Doussin, J.-F.,  
4 Crumeyrolle, S., Amarouch, N., Pichon, J.-M., Prévôt, A. S. H., Beekmann, M., and  
5 Schwarzenböeck, A. : Characterizing the impact of urban emissions on regional aerosol  
6 particles ; airborne measurements during the MEGAPOLI experiment, *Atmos. Chem. Phys.*  
7 *Discus.*, 13, 24 885–24 924, 2013.
- 8 Gilliland, A. and Abbitt, P. J. : A sensitivity study of the discrete Kalman filter (DKF) to initial  
9 condition discrepancies, *J. Geophys. Res.*, 106, 17 939, 2001.
- 10 Granier, C., Bessagnet, B., Bond, T., D'Angiola, A., Denier van der Gon, H. A. C., Frost, G. J., Heil,  
11 A., Kaiser, J. W., Kinne, S., Klimont, Z., Kloster, S., Lamarque, J.-F., Liousse, C., Masui, T.,  
12 Meleux, F., Mieville, A., Ohara, T., Raut, J.-C., Riahi, K., Schultz, M. G., Smith, S. J.,  
13 Thompson, A., Aardenne, J., Werf, G. R., and Vuuren, D. P. : Evolution of anthropogenic and  
14 biomass burning emissions of air pollutants at global and regional scales during the 1980-2010  
15 period, *Climatic Change*, 109, 163–190, 2011.
- 16 Guenther, A., Karl, T., Harley, P., Wiedinmyer, C., Palmer, P. I., and Geron, C. : Estimates of global  
17 terrestrial isoprene emissions using MEGAN (Model of Emissions of Gases and Aerosols from  
18 Nature), *Atmos. Chem. Phys.*, 6, 3181-3210, 2006.
- 19 Haeffelin, M., Angelini, F., Morille, Y., Martucci, G., Frey, S., Gobbi, G. P., Lolli, S., O'Dowd, C.  
20 D., Sauvage, L., Xueref-Rémy, I., Wastine, B., and Feist, D. G. : Evaluation of Mixing-Height  
21 Retrievals from Automatic Profiling Lidars and Ceilometers in View of Future Integrated  
22 Networks in Europe, *Bound.-Lay. Meteorol.*, 143, 49–75, 2012.
- 23 Hakami, A., Henze, D. K., Seinfeld, J. H., Chai, T., Tang, Y., Carmichael, G. R., and Sandu, A. :  
24 Adjoint inverse modeling of black carbon during the Asian Pacific Regional Aerosol  
25 Characterization Experiment, *J. Geophys. Res.*, 110, D14 301, 2005.
- 26 Hanna, S. R., Lu, Z., Christopher Frey, H., Wheeler, N., Vukovich, J., Arunachalam, S., Fernau, M.,  
27 and Alan Hansen, D. : Uncertainties in predicted ozone concentrations due to input  
28 uncertainties for the UAM-V photochemical grid model applied to the July 1995 OTAG  
29 domain, *Atmos. Environ.*, 35, 891–903, 2001.
- 30 Hansen, M. C. and Reed, B. : A comparison of the IGBP DISCover and University of Maryland 1 km  
31 global land cover products, *Int. J. Remote Sens.*, 21, 1365–1373, 2000.
- 32 Hansen, M. C., Defries, R. S., Townshend, J. R. G., and Sohlberg, R. : Global land cover  
33 classification at 1 km spatial resolution using a classification tree approach, *Int. J. Remote*  
34 *Sens.*, 21, 1331–1364, 2000.
- 35 Hauglustaine, D. A., Hourdin, F., Jourdain, L., Filiberti, M.-A., Walters, S., Lamarque, J.-F., and  
36 Holland, E. A. : Interactive chemistry in the Laboratoire de Meteorology Dyanmique general

- 1       circulation model: Description and background tropospheric chemistry evaluation, *J. Geophys.*  
2       *Res.*, 109, D04314, 2004.
- 3       Healy, R. M., Sciare, J., Poulain, L., Kamili, K., Merkel, M., Müller, T., Wiedensohler, A., Eckhardt,  
4       S., Stohl, A., Sarda-Estève, R., McGillicuddy, E., O'Connor, I. P., Sodeau, J. R., and Wenger,  
5       J. C. : Sources and mixing state of size-resolved elemental carbon particles in a European  
6       megacity : Paris, *Atmos. Chem. Phys.*, 12, 1681–1700, 2012.
- 7       Junker, C. and Liousse, C. : A global emission inventory of carbonaceous aerosol from historic  
8       records of fossil fuel and biofuel consumption for the period 1860-1997, *Atmos. Chem. Phys.*,  
9       8, 1195–1207, 2008.
- 10      Konovalov, I. B., Beekmann, M., Richter, A., and Burrows, J. P. : Inverse modelling of the spatial  
11      distribution of NO<sub>x</sub> emissions on a continental scale using satellite data, *Atmos. Chem. Phys.*,  
12      6, 1747–1770, 2006.
- 13      Konovalov, I. B., Beekmann, M., Burrows, J. P., and Richter, A. : Satellite measurement based  
14      estimates of decadal changes in European nitrogen oxides emissions, *Atmos. Chem. Phys.*, 8,  
15      2623–2641, 2008.
- 16      Lamarque, J.-F., Bond, T. C., Eyring, V., Granier, C., Heil, A., Klimont, Z., Lee, D., Liousse, C.,  
17      Mieville, A., Owen, B., Schultz, M. G., Shindell, D., Smith, S. J., Stehfest, E., Van Aardenne,  
18      J., Cooper, O. R., Kainuma, M., Mahowald, N., McConnell, J. R., Naik, V., Riahi, K., and van  
19      Vuuren, D. P. : Historical (1850-2000) gridded anthropogenic and biomass burning emissions  
20      of reactive gases and aerosols : methodology and application, *Atmos. Chem. Phys.*, 10, 7017–  
21      7039, 2010.
- 22      Liousse, C., Cachier, H., and Jennings, S. G. : Optical and thermal measurements of black carbon  
23      aerosol content in different environments: variation of the specific attenuation cross-section,  
24      sigma ( $\sigma$ ), *Atmos. Env.*, 27A, 8, 1203-1211, 1993.
- 25      Lohmann, U. and Feichter, J. : Global indirect aerosol effects : a review, *Atmos. Chem. Phys.*, 5,  
26      715–737, 2005.
- 27      McNaughton, C. S., Clarke, A. D., Howell, S. G., Pinkerton, M., Anderson, B., Thornhill, L.,  
28      Hudgins, C., Winstead, E., Dibb, J. E., Scheuer, E., and Maring, H. : Results from the DC-8  
29      Inlet Characterization Experiment (DICE) : Airborne Versus Surface Sampling of Mineral Dust  
30      and Sea Salt Aerosols, *Aerosol Sci. Tech.*, 41, 136–159, 2007.
- 31      Mendoza-Dominguez, A. and Russell, A. G. : Iterative Inverse Modeling and Direct Sensitivity  
32      Analysis of a Photochemical Air Quality Model, *Environ. sci. technol.*, 34, 4974–4981, 2000.
- 33      Menut, L., Bessagnet, B., Khvorostyanov, D., Beekmann, M., Blond, N., Colette, A., Coll, I., Curci,  
34      G., Foret, G., Hodzic, A., Mailler, S., Meleux, F., Monge, J.-L., Pison, I., Siour, G., Turquety,  
35      S., Valari, M., Vautard, R., and Vivanco, M. G. : CHIMERE 2013 : a model for regional  
36      atmospheric composition modelling, *Geoscientific Model Development*, 6, 981–1028, 2013.

- 1 Napelenok, S. L., Pinder, R. W., Gilliland, A. B., and Martin, R. V. : A method for evaluating  
2 spatially-resolved NO<sub>x</sub> emissions using Kalman filter inversion, direct sensitivities, and space-  
3 based NO<sub>2</sub> observations, *Atmos. Chem. Phys. Discuss.*, 8, 6469–6499, 2008.
- 4 Napelenok, S. L., Foley, K. M., Kang, D., Mathur, R., Pierce, T., and Rao, S. T. : Dynamic  
5 evaluation of regional air quality model's response to emission reductions in the presence of  
6 uncertain emission inventories, *Atmos. Environ.*, 45, 4091–4098, 2011.
- 7 Nenes, A., Pandis, S., and Pilinis, C. : ISORROPIA : A New Thermodynamic Equilibrium Model for  
8 Multiphase Multicomponent Inorganic Aerosols, *Aquat. geochem.*, pp. 123–152, 1998.
- 9 Parrish, D. D. : Critical evaluation of US on-road vehicle emission inventories, *Atmos. Environ.*, 40,  
10 2288–2300, 2006.
- 11 Peng, R. D., Bell, M. L., Geyh, A. S., McDermott, A., Zeger, S. L., Samet, J. M., and Dominici, F. :  
12 Emergency admissions for cardiovascular and respiratory diseases and the chemical  
13 composition of fine particle air pollution., *Environ. Health Persp.*, 117, 957–63, 2009.
- 14 Petetin, H., Beekmann, M., Sciare, J., Bressi, M., Rosso, A., Sanchez, O., and Ghersi, V. : A novel  
15 model evaluation approach focussing on local and advected contributions to urban PM<sub>2.5</sub>  
16 levels - application to Paris, France, *Geoscientific Model Development Discussions*, 6, 6391–  
17 6457, 2013.
- 18 Petzold, A., Ogren, J. A., Fiebig, M., Laj, P., Li, S.-M., Baltensperger, U., Holzer-Popp, T., Kinne,  
19 S., Pappalardo, G., Sugimoto, N., Wehrli, C., Wiedensohler, A., and Zhang, X.-Y. :  
20 Recommendations for the interpretation of "black carbon" measurements, *Atmos. Chem. Phys.*  
21 *Discuss.*, 13, 9485–9517, 2013.
- 22 Pouliot, G., Pierce, T.E., Denier van der Gon, H., Schaap, M., Moran, M., Nopmongkol, U. :  
23 Comparing emission inventories and model-ready emission datasets between Europe and North  
24 America for the AQMEII project. *Atmos. Environ.* 53, 4–14, 2012.
- 25 Schmidt, H., Derognat, C., Vautard, R., and Beekmann, M. : A comparison of simulated and  
26 observed ozone mixing ratios for the summer of 1998 in Western Europe, *Atmos. Environ.*, 35,  
27 6277–6297, 2001.
- 28 Schulz, M., Textor, C., Kinne, S., Balkanski, Y., Bauer, S., Berntsen, T., Berglen, T., Boucher, O.,  
29 Dentener, F., Guibert, S., Isaksen, I. S. A., Iversen, T., Koch, D., Kirkevåg, A., Liu, X.,  
30 Montanaro, V., Myhre, G., Penner, J. E., Pitari, G., Reddy, S., Seland, O., Stier, P., and  
31 Takemura, T. : Radiative forcing by aerosols as derived from the AeroCom present-day and  
32 pre-industrial simulations, *Atmos. Chem. Phys.*, 6, 5225-5246, 2006.
- 33 Sciare, J., d'Argouges, O., Sarda-Estève, R., Gaimoz, C., Dolgorouky, C., Bonnaire, N., Favez, O.,  
34 Bonsang, B., and Gros, V. : Large contribution of water-insoluble secondary organic aerosols  
35 in the region of Paris (France) during wintertime, *J. Geophys. Res.*, 116, D22203, 2011.

- 1 Skamarock, W. C., Klemp, J. B., Gill, D. O., Barker, D. M., and Powers, J. G. : A Description of the  
2 Advanced Research WRF Version 2, Tech. Rep., 2005.
- 3 Smit, R., Ntziachristos, L., and Boulter, P. : Validation of road vehicle and traffic emission models -  
4 A review and meta-analysis, *Atmos. Environ.*, 44, 2943–2953, 2010.
- 5 Tian, D., Cohan, D. S., Napelenok, S., Bergin, M., Hu, Y., Chang, M., and Russell, A. G. :  
6 Uncertainty Analysis of Ozone Formation and Response to Emission Controls Using Higher-  
7 Order Sensitivities, *J. Air Waste Manage.*, 60, 797–804, 2010.
- 8 Timmermans, R., Denier van der Gon, H.A.C., Kuenen, J.J.P., Segers, A.J., Honoré, C., Perrussel,  
9 O., Builtjes, P.J.H., and Schaap, M. : Quantification of the urban air pollution increment and its  
10 dependency on the use of down-scaled and bottom-up city emission inventories, *Urban  
11 Climate* 6 (2013) 44–62, 2013
- 12 Troen, I. B. and Mahrt, L. : A simple model of the atmospheric boundary layer ; sensitivity to surface  
13 evaporation, *Bound.-Lay. Meteorol.*, 37, 129–148, 1986.
- 14 Vautard, R., Martin, D., Beekmann, M., Drobinski, P., Friedrich, R., Jaubertie, A., Kley, D., Lattuati,  
15 M., Moral, P., Neininger, B., Theloke, J.: Paris emission inventory diagnostics from ESQUIF  
16 airborne measurements and a chemistry transport model, *J. Geophys. Res.*, 108, 8564, 2003.
- 17 Vestreng, V., Mareckova, K., Kakareka, S., Malchykhina, A., and Kukharchyk, T. : Inventory  
18 Review 2007 - Emission data reported to LRTAP Convention and NEC Directive, Tech. rep.,  
19 2007.
- 20 Vignati, E., Karl, M., Krol, M., Wilson, J., Stier, P., and Cavalli, F. : Sources of uncertainties in  
21 modelling black carbon at the global scale, *Atmos. Chem. Phys.*, 10, 2595–2611, 2010.
- 22 Virkkula, A., Ahlquist, N. C., Covert, D. S., Arnott, W. P., Sheridan, P. J., Quinn, P. K., and  
23 Coffman, D. J. : Modification, Calibration and a Field Test of an Instrument for Measuring  
24 Light Absorption by Particles, *Aerosol Sci. Tech.*, 39, 68–83, 2005.
- 25 Xu, W., Zhao, C., Ran, L., Deng, Z., Ma, N., Liu, P., Lin, W., Yan, P., and Xu, X. : A new approach  
26 to estimate pollutant emissions based on trajectory modeling and its application in the North  
27 China Plain, *Atmos. Environ.*, 71, 75–83, 2013.
- 28 Yu, H., Kaufman, Y. J., Chin, M., Feingold, G., Remer, L. A., Anderson, T. L., Balkanski, Y.,  
29 Bellouin, N., Boucher, O., Christopher, S., DeCola, P., Kahn, R., Koch, D., Loeb, N., Reddy,  
30 M. S., Schulz, M., Takemura, T., and Zhou, M. : A review of measurement-based assessments  
31 of the aerosol direct radiative effect and forcing, *Atmos. Chem. Phys.*, 6, 613–666, 2006.
- 32 Zhang, Q. J., Beekmann, M., Drewnick, F., Freutel, F., Schneider, J., Crippa, M., Prevot, A. S. H.,  
33 Baltensperger, U., Poulain, L., Wiedensohler, A., Sciare, J., Gros, V., Borbon, A., Colomb, A.,  
34 Michoud, V., Doussin, J.-F., Denier van der Gon, H. A. C., Haeffelin, M., Dupont, J.-C., Siour,  
35 G., Petetin, H., Bessagnet, B., Pandis, S. N., Hodzic, A., Sanchez, O., Honoré, C., and  
36 Perrussel, O.: Formation of organic aerosol in the Paris region during the MEGAPOLI summer

1 campaign: evaluation of the volatility-basis-set approach within the CHIMERE model, Atmos.  
2 Chem. Phys., 13, 5767-5790, doi:10.5194/acp-13-5767-2013, 2013.  
3 Zhou, X., Gao, J., Wang, T., Wu, W., and Wang, W. : Measurement of black carbon aerosols near  
4 two Chinese megacities and the implications for improving emission inventories, Atmos.  
5 Environ., 43, 3918–3924, 2009.